Practical sampling criteria for using delta channel width to estimate paleodischarge in the rock record

O.A. Prasojo[1,2*], A. E. van Yperen[3], T. B. Hoey[4], A. Owen[1] and R. Williams[1]

[1]*School of Geographical and Earth Sciences, University of Glasgow, University Avenue, Glasgow, G12 8NN, United Kingdom, o.prasojo.1@research.gla.ac.uk, Amanda.Owen@glasgow.ac.uk, Richard.Williams@glasgow.ac.uk*

[2]*Geoscience Study Program, Faculty of Mathematics and Natural Sciences (FMIPA), Universitas Indonesia, Depok 16424, Indonesia.*

[3]*Department of Geosciences, University of Oslo, 0316 Oslo, Norway, annavanyperen@gmail.com*

[4]*Department of Civil and Environmental Engineering, Brunel University London, Uxbridge, UB8 3PH, United Kingdom, Trevor.Hoey@brunel.ac.uk*

The following preprint is under review at **Journal of Sedimentary Research** by Prasojo, O.A., A. E. van Yperen, T. B. Hoey, A. Owen, and R. Wiliams.

ABSTRACT

Quantifying paleodischarge from geological field observations have been for decades, and remains, a key research challenge. Several paleodischarge scaling relationships have been developed for fluvial environments, such as BQART, Fulcrum and regional hydraulic geometry or for river deltas by precluding the role of wave and tide. In deltas where marine (wave, tide) energy causes bidirectional flow, the available paleodischarge scaling relationships are not applicable. Here, the spatial variability of distributary channel widths from a database of 114 global modern river deltas is assessed to understand the limit of marine influence on distributary channel widths. Compiling 4459 distributary channel width measurements enables improvements to distributary channel width-discharge scaling relationships specifically for river-, tide- and wave-dominated deltas. By bootstrapping the channel widths measured from modern deltas, the minimum number of width measurements needed to apply width-discharge scaling relationships to ancient deltaic deposits is estimated as 3 and 30 for upstream and downstream river-dominated deltas, consecutively, 6 for upstream part of tide-dominated deltas and 4 for wave-dominated deltas. This estimate will guide sedimentologists who often have limited numbers of distributary channel widths exposed in the rock record. Statistically significant width-discharge scaling relationships are derived for river- and wave-dominated deltas, with no significant relationships identified for tide-dominated deltas. To test the reliability of these improved width-discharge scaling relationships in the rock record, paleodischarges were estimated for the well-studied Cretaceous lower Mesa Rica Formation, USA. Comparison of these results with the more complex Fulcrum method suggests that these new scaling relationships are accurate. Hence these scaling relationships obtained from modern deltas can be applied to the rock record, and this approach requires less, and easier to measure, data inputs than previously published methods.

INTRODUCTION

Sedimentary deposits provide an important archive of interactions between tectonic and climate activity in deep geological time (Sharman et al., 2019). However, reconstructing paleodrainage settings from sedimentary deposits remains a challenge (Nyberg et al., 2021). Specifically, estimating rates of key earth surface processes such as sediment flux and paleodischarge has been a key research challenge for decades (Whittaker, 2012; Lyster et al., 2021). Estimating paleodischarge plays an important role in quantifying sediment transport capacities and volumes (Allen et al., 2013; Holbrook and Wanas, 2014; Lin and Bhattacharya, 2017; Sharma et al., 2017), understanding the scale of ancient catchments (Bhattacharya and Tye, 2004; Bhattacharya et al., 2016; Eide et al., 2018; Lyster et al., 2020), and investigating paleoclimate impact on paleochannel hydrology (Duller et al., 2010; Whittaker et al., 2011; Castelltort et al., 2012; Hampson et al., 2013).

Most of the models proposed to estimate paleodischarge, such as BQART (Syvitski and Milliman, 2007), the Fulcrum model (Holbrook and Wanas, 2014; Bhattacharya et al., 2016), or regional hydraulic geometry (Syvitski & Milliman, 2007; Davidson & North, 2009; Holbrook & Wanas, 2014; Bhattacharya et al., 2016) are suitable to purely unidirectional fluvial environments since they do not consider the influence of marine energies that may alter the unidirectionality of river current (Syvitski and Milliman, 2007; Davidson and North, 2009; Holbrook and Wanas, 2014; Bhattacharya et al., 2016). The BQART model incorporates a scaling relationship between the water discharge (Q) and catchment area (A) from the 63% of the world's river discharge ($Q = 0.075A^{0.8}$) to estimate sediment flux, assuming that these two variables are partly independent (Syvitski and Milliman, 2007). Consequently, applying BQART to ancient sedimentary systems needs robust paleogeographic reconstructions to estimate the paleocatchment area, itself challenging to reconstruct from the rock record (Nyberg et al., 2021). Similar to the BQART model, the Fulcrum model needs several parameters that are challenging to extract from rock records such as bankfull depth and width, estimated paleoslope, estimated bankfull Shield's stress and the dimensionless Chezy friction coefficient (Holbrook and Wanas, 2014; Bhattacharya et al., 2016; Brewer et al., 2020).

On the other hand, a new rock-record focused channel width-discharge scaling relationship for river deltas (Prasojo et al., *in review*) precludes the role of wave and tide, assuming distributary channels contain only unidirectional river currents. Another model, WBMSed, was recently applied for estimating the global river deltas discharges (Cohen et al., 2013; Nienhuis et al., 2020). Although WBMSed produced fairly reasonable prediction of several rivers in the USA and predictions were comparable with the BQART model, WBMSed model does not take into account the influence of marine energy that can significantly alter the geometry of delta distributary channels of river deltas (Nittrouer, 2013; Chatanantavet et al., 2012; Lamb et al., 2012; Fernandes et al., 2016; Ganti et al., 2016; Martin et al., 2018; Chadwick et al., 2019, 2020; Gugliotta & Saito, 2019).

It is expected that channel width scaling relationships in deltas weaken with more significant marine energy influence (wave, tide, longshore currents) due to bidirectional flow and channel deflection in more distal parts of delta plains (Besset et al., 2017). The presence of large tidal, wave energy or backwater-controlled flow regimes also significantly alters the geometry of delta distributary channels, hence directly weakening scaling between channel width and discharge (Fig. 1). The effect on channel geometry, including narrowing and deepening, due to marine influences has also been demonstrated (Chatanantavet et al., 2012; Lamb et al., 2012; Nittrouer, 2013; Fernandes et al., 2016; Ganti et al., 2016; Martin et al., 2018; Gugliotta and Saito, 2019;

Chadwick et al., 2019; Chadwick et al., 2020). To consider the marine influence on width-discharge scaling relationship, the break in distributary channel morphology (i.e. channel width; Sassi et al., 2012) that classifies delta plains into upstream, assuming no marine influence, and downstream, marine-influenced parts needs to be identified for river-, tide- and wave-dominated deltas. This provides an opportunity to create a more accurate discharge/paleodischarge estimation from river deltas.

This study aims to assess the spatial variability of distributary channel widths from a database of 114 global river deltas to improve channel width-discharge scaling relationships, in which a clear break in distributary channel widths is identified that separates upstream and downstream parts of the delta. The downstream parts are characterised by channels which widen towards the sea, whereas in upstream parts channel widths remain broadly constant between successive bifurcations to the delta apex. A total of 4459 distributary channel widths from the 114 river deltas were measured from the delta apex, or first avulsion point, to the shoreline.

In contrast with modern river deltas on which distributary channel widths can be measured directly from satellite images or in the field, ancient delta deposits typically have very limited distributary channel exposure or preservation hence the width cannot be determined directly. In this study we apply a bootstrap method to the large global modern delta dataset (N = 4459) to simulate the optimum number of measurements needed to estimate paleodischarge from a deltaic deposit. By applying bootstrapping, we provide a guideline for the minimum number of width measurements that are needed from the rock record to reliably use the newly established channel width-discharge scaling relationships.

Overall, the aims of this study are: (1) to identify any morphological break or down-dip spatial variation of delta distributary channel widths; (2) to improve channel width-discharge scaling relationships for delta channels based on analysing data with regard to down-delta breaks in channel width; (3) to apply a bootstrap method to the modern delta data to simulate the limited number of data points usually available from the rock record; and, (4) to compare the results from the improved channel width-discharge scaling relationships with those obtained using the Fulcrum method.

METHODS

Dimensionless distributary channel widths of river deltas

The active channel width of distributary channels from 114 deltas (including 97 river-dominated deltas, 7 tide-dominated deltas, and 10 wave-dominated deltas) across different climate regions were measured from Landsat 5 satellite images in Google Earth Engine (GEE). The earliest (~2009) and the least cloudy images were chosen for image clarity purposes, as well as to minimize the influence of ongoing anthropogenic activities such as embankment construction. Distributary channel widths were measured manually along all the identifiable distributary channels seen on Landsat 5 (minimum channel width of 100 m) from the delta apex to the shoreline. The delta apex is assumed to be the present-day most landward bifurcation point observed on satellite images (Ganti et al., 2016). Where deltas have a single channel, the delta apex is associated with the valley exit point from its Digital Elevation Model (DEM) (Hartley et al., 2017). To enable comparison of channel widths measured from different sized deltas, we use the semicircular grid s/L method (Sassi et al., 2012) to ensure even spacing of measurements, where s represents the along-channel distance from the delta apex, and L is the along-channel distance of the longest distributary channel to the delta apex (Fig. 2). The semicircular grid allows measurement of multiple distributary channels located at the same dimensionless distance from the apex point. The grid resolution is ~10 times the river channel width at the delta apex to maintain consistent dimensionless distance and data collection frequency across deltas of varying size. As an example, if a delta has a 100 m wide channel at its apex, the semicircular grid will have diameters of 1, 2, 3... km until the grid covers the entire delta plain (Fig. 2). Thus, channel width is measured at *s/L* = 1, 0.9, 0.8... , 0.1, 0. Only channel widths along definite distributary channels (N = 4459) were included to exclude the influence of non-riverine influences in delta systems, such as tidal creeks. Where distributary channels contain mid-channel bars, the width of the wider channel was measured (inset Fig. 2).

Deltas were identified based on protrusion of their visible deposits beyond their lateral shorelines (Caldwell et al., 2019). They were then classified as river-, wave- or tide-dominated, based on (Nienhuis et al., 2020) dataset. Morphologically, river-dominated deltas are characterized by multiple/single elongated distributary channels that protrude beyond the shoreline and subaerial mouth bar deposits (Olariu and Bhattacharya, 2006). Wave-dominated deltas have linear shorefaces and mouth bars modified by wave action. In most cases, the number of distributary channels in wave-dominated delta is limited (Bhattacharya and Giosan, 2003; Bhattacharya and Tye, 2004; Li et al., 2011). Tide-dominated deltas are characterized by a funnel-shaped distributary channels with abundant tidal creeks on adjacent delta plains. We simplify the classification into the three end-members of (Galloway, 1975) same as (Nienhuis et al., 2020) but acknowledge other delta classifications (Li et al., 2011; Vakarelov and Ainsworth, 2013; Lin and Bhattacharya, 2021).

Dimensionless distance was plotted against dimensionless channel width (W^*) for each delta type. Dimensionless distance is defined as *s/L* consistent with the semicircular grid (Fig. 2) that originates at the delta apex. Dimensionless width (W^*) is defined as W/W_A where W is channel width and W_A is the channel width at the delta apex. Subsequently, down-dip changes in dimensionless channel widths form the basis of classifying the delta plain into 'upstream' and 'downstream' parts. To aid recognizing any contrasts between 'upstream' and 'downstream' distributary channel width patterns, the non-parametric Kruskal-Wallis one-way analysis of variance test was conducted. Data binning of 10% of original data was later used as the basis of 'upstream-downstream' classification due to its proper representativity of the overall data without producing significant bias (see Supporting Information and Fig. S1 for details). The classifications between 'upstream' and 'downstream' parts were then the basis of running a bootstrap method on to the dataset.

Bootstrapping the distributary channel width distribution from modern river deltas

Bootstrapping was undertaken to assess the impact of a limited sample size that may be retrieved from the rock record. This is a common resampling method that has been widely used in field studies with limited sample size (Cheng and Yeager, 2007; Cui et al., 2017; Debchoudhury et al., 2019). Bootstrapping involves repeat resampling of the original dataset with replacement (Efron, 1982; Efron, 2007). Resampling is repeated *B* times (*B* is typically a power of 10, e.g. 10, 100, 1000…) to transform a small number of measurements into a much larger sample size to improve the validity of statistical results obtained from analysing the data (Cui et al., 2017).

In this study, rather than increasing the sample size from a large number of measured channel widths from modern river deltas, bootstrapping was used to reduce this sample size to simulate the typically small number of distributary channel widths that can be measured from outcrops. Bootstrapping used from 100% to 3% of the original number of distributary channel widths measured from modern deltas. Standard errors of these re-sampled data sets were calculated and plotted against the number of samples to show the distribution of standard errors for different sample sizes. Standard error (S) is defined in Equation 1 as:

$$S = \frac{\sigma}{\sqrt{N}} \tag{1}$$

with σ representing the standard deviation of channel widths (m) and N the number of measurements in the sample. The plots simulate errors that may be encountered by measuring small numbers of distributary channel widths in the rock record. The relationships between sample size and standard error can be used to inform sample size determination for field studies as well as to quantify the uncertainties in measurements. Percentile standard errors were calculated to understand how the distribution of measured distributary channel widths influences the shape of the distribution of synthetic samples of different size. This analysis was designed to overcome the small sample sizes from ancient field measurements through analysis of a large contemporary data set; the influence of sample size on estimates of width is known for a normal distribution through equation (1), but using a large real data set provides understanding of the influence of the shape of the underlying distribution on the results.

Improving delta width-discharge scaling

To improve the previously available scaling relationships between channel width and total river discharge for river deltas (Prasojo et al., *in review*), we apply the same method to the scaling relationship between distributary channel width and total discharge by correlating the median channel widths of distributary channels for each delta to its consecutive bankfull discharge using an ordinary least square (OLS) regression. We expand width-discharge scaling from river-dominated deltas to also include wave- and tide-dominated deltas based on (Nienhuis et al., 2020) dataset and reclassify each delta type based on down-dip (down-delta) changes in dimensionless distributary channel width, as explained above. This approach provides refined width-discharge scaling relationships that take into account the marine influence on distal distributary channel widths.

All scaling relationships assume a power law relationship (i.e. linear on a log-log plot) between input river discharge and channel width (Leopold and Maddock, 1953). Hence, OLS regressions were then used to calculate relationships between these two variables. Median values of measured channel width (W_{med}) from each delta were plotted against the respective bankfull discharge values (Q_2). Median channel widths were preferred to means due to the width distributions being non-Gaussian, such that the median is more representative of the whole channel width population. Using the median also reduces the influence of extreme values, so reducing the need to identify and exclude channels where tidal influence controls their width. Further, as it is challenging to detect how many distributary channels were active at the same time in the rock record, using one median value of channel width per delta helps in minimizing the effect of this difficulty but explicitly assesses the statistical uncertainty associated with the number of measurements that could be made.

Bankfull discharge is widely considered as the flow that controls channel geometry in alluvial rivers (De Rose et al., 2008; Haucke and Clancy, 2011; Gleason, 2015), although other factors also affect this geometry. Bankfull discharge is estimated from daily discharge data using Q_2, where 2 is the recurrence interval (years) of the discharge (see also Eaton, 2013; Jacobsen and Burr, 2016; Morgan and Craddock, 2019). Calculations used the Flow Analysis Summary Statistics Tool (‘*fasstr*’) package for R (https://github.com/bcgov/fasstr). For some sites only monthly discharge data were available, from which daily equivalent Q_2 values were obtained using a climate-classified transformation (Supporting Information and Fig. S2; (Beck et al., 2018). The discharge dataset was extracted from the Global Runoff Data Centre (GRDC), using the river gauges located closest to the delta apex.

Applying width-discharge scaling relationships the rock record

To test the reliability of the scaling relationships produced in this study for the rock record, we utilized ~400 km transects of the Cenomanian Mesa Rica (Dakota Group, USA) exposed along an overall NNW- to SSE-oriented depositional profile in southeast Colorado and northeast New Mexico (Holbrook, 1996; R.W. Scott et al., 2004; Oboh-Ikuenobe et al., 2008; van Yperen et al., 2019; van Yperen et al., 2020). In east-central New Mexico, the Mesa Rica is subdivided into lower, middle and upper units (R.W. Scott et al., 2004; van Yperen et al., 2019). The up-dip reaches of the lower Mesa Rica depositional system consist of single-story trunk channel deposits that form sheet like geometries (Holbrook, 1996; Holbrook, 2001). A down-dip transition from fluvial to deltaic deposits occurs at the northwestern rim of the Tucumcari sub-basin (Western Interior Basin). Here, the lower Mesa Rica consists of coalesced mouth-bar deposits overlain by amalgamated sandy distributary-channel deposits indicative of a river-dominated delta (van Yperen et al., 2019; van Yperen et al., 2020). During the Cretaceous, the Mesa Rica was located at ~35°N latitude, with a warm and humid climate (Chumakov et al., 1995).

Distributary channel width measurements from the lower Mesa Rica consist of 13 data points distributed down-dip throughout the depositional system, from proximal (up-dip of the delta apex) to distal (Fig. 3; Table 1). The distributary channel widths were plotted as dimensionless width (W^*) and dimensionless distance down-dip (s/L), assuming that the proximal channel width is represented by the width at the delta apex. The bootstrap method was then applied to this rock record dataset with a range of repetition numbers (B = 1, 100, 1000, 10000). Subsequently, paleodischarges were estimated using the empirical relationships generated in this study from modern deltas. To test the reliability of these calculated paleodischarge estimates, we also estimated paleodischarge using the Fulcrum method (Holbrook and Wanas, 2014). See Supporting Information for details of the paleodischarge calculation using the Fulcrum method (Table S1).

The Fulcrum method and the width-discharge scaling relationships developed in this study share the assumptions of the erosional geometry that defines the shape of the channel infill being in equilibrium with water discharge, and the paleochannel position being fixed. Preservation of a channel fill deposit requires aggradation, hence non-equilibrium.

RESULTS

Down-dip changes in distributary channel widths

Description: Dimensionless widths from the distributary channels of 97 river-dominated deltas (Fig. 4A; Table S2) show a gradual downstream decrease towards $s/L = 0.1$. A substantial increase in $W*$ with higher variance occurs at the shoreline, $s/L = 0$, in comparison to up-dip counterparts. The abrupt change in $W*$ distinguishes the upstream from the downstream part of the delta plain in these river-dominated deltas. The non-parametric Kruskal-Wallis one-way analysis of variance test corroborates classification between the upstream ($1 \leq s/L \leq 0.1$) and the downstream ($s/L = 0$) parts of distributary channel widths with $p < 0.05$.

Tide-dominated deltas (N = 7; Table S2) in this study show a gradual increase of $W*$ towards the shoreline (Fig. 4B). In the upstream part ($1 \leq s/L \leq 0.5$), spatial variation is apparent in $W*$. However, this variation lies within the interquartile ranges of the data and may not be significant. In contrast, a substantial increase of $W*$ occurs at $s/L<0.5$ (Fig. 4B); this abrupt change in dimensionless channel is defined to mark the transition between upstream and downstream parts (Fig. 4E). Statistical significance test (Kruskal-Wallis test) corroborates the significance of upstream-downstream parts classification of $W*$ with $p < 0.05$.

The wave-dominated deltas (N = 10; Table S2) show consistent dimensionless distributary channel width across the delta plain (Fig. 4C), with an abrupt decrease at $s/L \sim 0.6$ (Fig. 4C). Nonetheless, there is no significant change in $W*$ between $1< s/L <0.7$ and $0.6< s/L <0$ (Kruskal-Wallis test; $p > 0.5$), corroborating that distributary channel widths in wave-dominated deltas remain relatively constant downstream.

Interpretation: The abrupt and substantial increase in $W*$ at $s/L = 0$ in river-dominated deltas can be related to mouth-bar processes (Olariu and Bhattacharya, 2006). Mouth-bar deposition is mainly caused by a decrease in sediment carrying capacity due to the decreasing velocity of the river flow when it enters the standing body of seawater (Edmonds and Slingerland, 2007). Sediment carried by the distributary channels tends to be deposited along channel levees and also in a subaqueous mouth-bar that induces bifurcation as it grows (Fig. 4D, G; ‘phase 2’ of (Olariu and Bhattacharya, 2006)). As channels become shallower due to mouth bar growth, bank erosion accelerates so increasing the channel width at the river mouth, $s/L = 0$, as shown in this study. The data in this study shows similar channel widening at distributary mouths of river-dominated deltas due to this phenomenon.

In tide-dominated deltas, the downstream increase of $W*$ downstream of $s/L<0.5$ is progressive rather than abrupt and results from the impact of tidal energy. The interaction between the unidirectional river flow and tidal currents within the standing body of seawater produces an interplay of physical (river, tides, waves), chemical (salinity), and biological (bioturbation) processes, seen in both modern and ancient systems (Dalrymple and Choi, 2007). To separate the upstream and downstream parts of tide-dominated deltas, we utilized the subzone classification of the fluvial-to-marine transition zone (FMTZ) (Gugliotta et al., 2016). The onset of the substantial increase of channel width downstream coincides with the boundary between the ‘fluvially-dominated, tidally-influenced’ and ‘tidally-dominated, fluvially-influenced’ zones. This boundary represents the sedimentological landward limit of tidal dominance. In the ‘tidally-dominated, fluvially-influenced’ zone, the role of river energy is predominantly as the sediment supplier. Additionally, the boundary position will shift landward and seaward due to the changes in the fluvial discharge (Dashtgard et al., 2012; Dalrymple et al., 2015; Jablonski and Dalrymple, 2016; Gugliotta et al., 2016) and cyclic fluctuations of tidal modulation (Allen et al., 1980; van den Berg et al., 2007; Dalrymple and Choi, 2007; Kravtsova et al., 2009). Even though each delta distributary channel could have a different FMTZ location, the boundary between the ‘fluvially-dominated, tidally-influenced' and 'tidally-dominated, fluvially-influenced' zones consistently show statistically significant change in channel width at $s/L = 0.45$ globally (Fig. 4B).

Wave-dominated deltas occur in coastal settings with strong longshore currents that redistribute sediment away from the river mouth, producing different updrift and downdrift characteristics (Fig. 4F) (Bhattacharya and Giosan, 2003). Longshore wave energy tends to produce a single dominant distributary channel in these deltas (Korus and Fielding, 2015). Increasing the long-term wave energy relative to fluvial input will increase longshore sediment dispersal, thereby reducing the rate of channel-belt aggradation and associated seaward extension and increasing the avulsion timescale by a factor of approximately 50 (Swenson, 2005). The increase in avulsion timescale, hence reduction in avulsion frequency, limits a distributary network growth like in river- or tide-dominated deltas. Also, strong longshore wave energy tends to sweep the mouth bar early deposit, hampering channel splitting due to mouth bar deposition. This absence of distal channel splitting explains the observed constant W^* from wave-dominated deltas from our global dataset (Fig. 4C). There is consequently no differentiation between upstream and downstream parts of wave-dominated deltas.

Bootstrapping estimation of sample standard error

Description: The standard error distributions produced by the bootstrapping dimensionless distributary channel widths in all delta types show a monotonic decrease with increasing number of measurements (Fig. 5A-E). The standard errors of dimensionless width (S_{w*}) estimates are significantly lower in the upstream parts of river-dominated deltas than in any of the other data sets (y-axis values in Fig. 5A-E). In contrast, the downstream parts of both river- and tide-dominated deltas consistently show the highest standard error values.

The implication of these low mean standard errors in the upstream parts of river-dominated deltas, where standard error is consistently < 0.1 when N exceeds 30 (using B=10; Fig. 5A), is that the standard error remains low (S_{w*}~0.2) with as few as three measurements (inset Fig. 5A). In the downstream part of river-dominated deltas, high variance of 75 measured dimensionless channel widths leads to high standard errors (S_{w*} up to ~1) from 1000 bootstrap replications (B) (Fig. 5B). The standard error reduces to 0.5 only when N is about 30 (inset Fig. 5B).

In tide-dominated deltas, upstream standard errors are lower (S_{w*}~0.4) than downstream (S_{w*}~2) from 1000 bootstrap replications (Fig. 5C, D). Only 6 data points are required to reduce the standard error (S_{w*}) to 0.5 (inset Fig. 5C). The standard errors in downstream parts of tide-dominated deltas remain high for all sample sizes (i.e. S_{w*} = 1.5-3) (inset Fig. 5D).

In wave-dominated deltas the standard error reduces monotonically from 1000 bootstrap replications (Fig. 5E). Using five data points, S_{w*}~0.4 (inset Fig. 5E), and increasing the number of samples to 60 only reduces the standard error (S_{w*}) to 0.2.

The distributions of mean standard errors for each percentile are plotted in Fig. 5F-K. All the delta types consistently show asymmetry in standard errors for equivalent percentiles (P5-P95; P16-P84; P25-P75) around their respective P50 standard error distributions. Tide-dominated deltas show the largest difference between the percentiles, reflecting the skewed distribution of dimensionless distributary channel widths, while the upstream parts of river-dominated deltas reflect a lower skew in this distribution of dimensionless distributary channel widths.

Interpretation: In the upstream section of river-dominated deltas where the unidirectional river current is dominant, changes in distributary channel patterns produced the least standard error compared to other delta types. While on the other extreme, the lack of a dominant unidirectional river current (e.g. in downstream part of tide-dominated deltas) shows the highest standard error distribution (Fig. 5D) due to the higher variance in the measured distributary channel widths. As shown in this study, when the river current becomes influenced by the large tidal or backwater-related processes that weaken the unidirectionality of river current, the standard error becomes higher (e.g. downstream part of tide-dominated deltas in Fig. 5C). On the other hand, the smaller the standard error, the less the influence of tidal or other backwater-related processes (e.g. upstream part of river-dominated deltas in Fig. 5A).

The positive skewness in dimensionless channel widths in all delta types and locations has also been reported from fluvial outcrops and seismic sections (Colombera et al., 2019). This suggests that all consecutive statistical approaches on channel width measurement from river deltas should be treated with having non-normal distributions.

Improving delta hydraulic geometry models

Description: Log-log plots (Fig. 6A-E) show power law relationships between the bankfull discharge of the river upstream of the delta (Q_2) and median channel width (W_{med}) with Fig. 6F showing the power law relationship between the overall measured distributary channels (W) and the bankfull discharge (Q_2). River- and wave- dominated deltas show how hydraulic geometry theory (i.e. a significant, p<0.05, positive power law relationship between channel width and discharge) applies to these two delta types (Fig. 6A,B,E). However, in tide-dominated deltas negative power law relationships occur (Fig. 6C,D), although these are not significant due to small sample sizes. Correlations are high in the upstream parts of river- dominated, $Q_2 = 5.82W^{1.11}$ (R^2 = 0.53; s=0.13), and wave-dominated deltas, $Q_2 = 0.42W^{1.48}$ (R^2 = 0.68; s=0.36) (Fig. 6A, E). Standard error from regression (s) is higher in wave-dominated deltas due to smaller sample sizes than the river-dominated deltas and R^2 is lower (0.17; s=0.2) on the downstream part of river-dominated deltas.

Slope tests were conducted to identify the difference between upstream-downstream regression lines of bankfull discharge (Q_2) and median channel width (W_{med}) from river- and tide-dominated deltas. We also compared the regression lines from each delta type to the global W-Q_2 equation shown in Fig. 6F. The slope tests show $p < 0.05$ for all regressions when being compared to both the global and between upstream-downstream parts.

Interpretation: The scatter in median width-discharge data (Fig. 6) increases (and, although affected by sample size, so does the regression standard error s) where marine energy (tides, longshore currents, waves) is greater, and that this energy directly impacts distributary channel width. Tidal energy obstructs the down-delta flow and causes distal widening, reflected in the distribution of distributary channel widths (Fig. 4B) and the standard errors of width estimates derived from samples (Fig. 5C,D).

Mouth-bar deposition also affects channel width in the downstream part of river-dominated deltas (Fig. 4A, 5B, 6B), as noted by (Olariu and Bhattacharya, 2006). Subaqueous mouth-bar deposition triggers a drop in transport capacity due to jet expansion and flow deceleration, hence producing relatively wider distributary channels than the upstream part. Upstream of any influence of marine energy, channel width is directly related to the scale of the supplying river system (Fig. 4A,C, 5A,E, 6A,E). Longshore wave energy and sediment redistribution does not significantly affect the distributary channel width in wave-dominated deltas (Fig. 4C), thus river discharge retains a significant influence and a statistically significant width-discharge scaling relationship is found (Fig. 6E). Power law relationships between W_{med} and Q_2 produced here do not allow prediction of the discharge/paleodischarge value of a single distributary channel but enable calculation of the total riverine discharge that contributes sediment to builds the delta plain. These results imply that the principles of hydraulic geometry are applicable to river- and wave-dominated deltas but not to tide-dominated deltas. Since the slope tests show significant difference between upstream-downstream and between each delta type to the global W-Q_2 scaling, upstream-downstream and global scaling produced in this study could not be used interchangeably.

Testing width-discharge scaling relationships on a rock record case study

Description: In total, 13 measured distributary channels were measured at locations across the delta identified in the lower Mesa Rica Formation (Fig. 7A; Table 1). No significant changes occur in channel widths downstream (i.e. Wilcoxon test $p > 0.05$, variance test $p > 0.05$). The whole sample shows a bimodal distribution (Fig. 7B). As the proximal zone contains only one measurement, which is from a trunk channel, we can neglect this zone because it is part of the fluvial system and not a part of the delta plain. Consequently, we use the distributary channel widths measured from the transitional (N=5) and the distal zones (N=7) which show skewed distributions (Fig. 7B). Applying the bootstrap method on dimensionless distributary channel widths measured on the transitional and distal parts produced low standard error (S_{w*} ~0.13-0.18) from 1000 bootstrap replicates (B) (Fig. 7C). The standard error remains low (~0.18) when using only the seven measurements from the lower Mesa Rica (Fig. 7C).

Interpretation: The delta front sandstone bodies of the lower Mesa Rica are interpreted to be deposits from a river-dominated setting (van Yperen et al., 2019). The down-dip decreasing values of measured distributary channel widths are similar to downstream trends in channel width from upstream parts of modern river-dominated deltas (Fig. 4A). To calculate paleodischarge from the distributary channels of the lower Mesa Rica, the median channel width of 12 measured distributary channel widths, 109 m, was input to the hydraulic geometry equation obtained above for the upstream part of river-dominated deltas, $Q_2 = 5.8W^{1.11}$ (Fig. 6A) giving $Q_2 = 1010 \pm 100$ m^3/s (i.e. ± showing error propagation from upstream part of river-dominated delta regression line and measured channel widths from Lower Mesa Rica Formation). The Fulcrum method, based on trunk channel deposits, produces a range of Q_2 = 1085-1392 m^3/s (see Supporting Information for details). These values overlap, although the central estimate that we obtained is 10% lower than from the Fulcrum method.

DISCUSSION

Down-dip changes in distributary channel width in modern and ancient deltas

Modern deltas perspective.---From 4459 measured channel widths across different delta types in various climate regions, it is shown that marine processes (waves, tides, longshore currents) influence the distributary channel widths differently according to the type of delta. In river-dominated deltas, the data consistently show that channel width decreases down-dip before a sharp increase at the shoreline due to mouth-bar deposition (Fig. 4A). Olariu and Bhattacharya (2006) provide a similar case study from the Trovimovskaya River, a distributary channel from the river-dominated Lena delta. In tide-dominated deltas, tides lead to increased channel widths up to around half of the distance from the shoreline to the delta apex, consistent with observations made for several geometrical properties (channel curvature, width/depth ratio, bed level, bifurcation order) in the Kapuas, Mahakam and Mekong modern deltas (Sassi et al., 2012; Kästner et al., 2017; Gugliotta et al., 2019). Longshore currents in wave-dominated deltas lead to lateral sediment redistribution parallel to the shoreline and formation of a cuspate geometry, rather than in the down-dip direction. However, these marine processes do not produce statistically significant down-dip change of channel widths in wave-dominated deltas. Understanding the boundaries between upstream and downstream sections across different delta types is imperative in applying the hydraulic geometry models we proposed from the modern system. However, finding the upstream-downstream patterns from deep time delta deposits will remain challenging yet interesting to be tested, considering the fact that hydraulic geometry behaves significantly different ($p < 0.05$) in each delta type.

Ancient delta perspective.---The study has demonstrated both the overall controls over channel width and down-dip patterns of distributary channel widths from modern systems and how this information can be used in interpreting ancient systems. Limited exposure often prevents the collection of large numbers of channel width measurements. The 4459 measurements from modern distributary channels allow us to simulate the consequences of sampling limited numbers of distributary channel widths in the rock record. Using bootstrapping, we simulate standard error distributions that may be expected when limited numbers of channel widths are able to be measured from outcrops. If it is possible to identify the relative down-delta position of measurements, specific width-discharge relationships are available and the uncertainties in estimating discharge can be determined. As well as quantifying uncertainty, these results can be used in field work planning by enabling dynamic estimation of the number of samples required as data are gathered.

The example from the lower Mesa Rica provides an example of how the down-dip pattern of distributary channel widths could be recognized from the rock record and compared with modern systems. By having the down-dip pattern, the same bootstrapping method to reduce the number of samples could produce a range of standard error values that could be expected from the rock record (Fig. 7C). By recognizing the down-dip pattern along with the context of the depositional setting through the sedimentary structure and facies distribution, upstream part of river-dominated delta was then used to estimate the paleodischarge value from this formation due to their similar down-dip patterns. The other scaling relationships proposed in this study can be applied to deltaic outcrops that have evidence for different dominant energies (e.g. wave- or tide-dominated deltas).

Standard error distribution of deltas distributary channel widths.---Fig. 5 shows the relationships between number of measured distributary channel widths and the mean standard error using bootstrapping method. In river- and wave-dominated deltas, low standard errors of dimensionless width occur (Fig. 5A,B,E). These low errors imply that reliable estimates of median channel width (i.e. depends on the aims of the study) can be obtained from a small number of measurements. However, for tide-dominated deltas it is challenging to produce reliable width estimates that can be related to input river discharge due to the significant influence of tidal energy on channel form. Even with 30 data points in the downstream part of tide-dominated deltas, the standard error of dimensionless width remains high (S_{w*}>1). Thus, caution should be taken when applying tide-dominated delta discharge-width scaling relationship from either the modern system or the rock records.

Channel width distributions across all delta types and climate regions are skewed, implying that mean distributary channel width may not be statistically representative (Fig. 5G-K) and that median values are better representative values of channel width. This has implications for the application of other scaling relationships where small sample sizes are available; many such relationships are used including those with catchment area, meander wavelength, channel sinuosity, total river-atmosphere carbon dioxide flux, mean and peak discharge, and sediment transport mode (Leopold and Maddock, 1953; Bridge and Mackey, 1993; Bhatt and Tiwari, 2008; Gleason et al., 2018; Allen and Pavelsky, 2018; Frasson et al., 2019; Dunne and Jerolmack, 2020; Lyster et al., 2021).

Comparing width-discharge relationships with the Fulcrum method.---Bankfull discharges estimated from the width-discharge relationships in this study lie within 10% of those obtained using the Fulcrum method, and their uncertainty ranges overlap significantly, suggesting that these approaches are consistent. Our method uses only a single parameter, channel width, whereas the Fulcrum method uses estimates of bankfull channel depth and width, paleoslope, mean bedform height and wavelength (Bridge and Tye, 2000; Leclair and Bridge, 2001; Holbrook and Wanas, 2014; Trampush et al., 2014). As well as relying on a single input parameter, where stratigraphic and/or paleoclimate data are available, our method allows estimates to be tailored to delta type, the along-dip location of the measured widths, and climate zone.

Further data will allow systematic down-dip scaling relationships to be developed for other channel types, such as tidal creeks, and may enable further differentiation of delta types. Similar work has been undertaken in modern estuaries (Diefenderfer et al., 2008; Gisen and Savenije, 2015) and tide-influenced deltas (Sassi et al., 2012). Improved understanding of the system scale is important to further source-to-sink analyses and hence improve volumetric assessment of resource reservoirs, and carbon capture and storage facilities, as well as deducing climate and tectonic forcing and refining paleohydraulic reconstructions (Montgomery and Gran, 2001; Merritt and Wohl, 2003; Bhattacharya and Tye, 2004; Brardinoni and Hassan, 2006; Wohl and David, 2008; Davidson and Hartley, 2010; Eaton, 2013).

Limitations of applying modern delta scaling relationships to the rock record.---We show that distributary channel width (W_{med}) scales with input river bankfull discharge (Q_2) from our global dataset (Fig. 6F). However, this study provides empirical evidence of how deltaic width-discharge scaling relationships start to weaken with the increasing influence of marine processes that directly influence hydraulic and sediment processes (Fig. 6A-E). Scaling relationships derived from the upstream parts of river-dominated deltas, from which marine influence is largely absent, show strong statistical correlation between median channel width and input river discharge ($R^2 = 0.53$; $p < 0.05$) (Fig. 6A). The correlations are weaker ($R^2 = 0.17$; $p < 0.05$) for downstream parts of river dominated deltas and stronger (R^2 = 0.68; $p < 0.05$) for wave-dominated deltas and becomes statistically insignificant in the upstream part of tide-dominated deltas (R^2 = 0.04; $p > 0.05$), and downstream tide-dominated deltas (R^2 = 0.01; $p > 0.05$) (Fig. 6A-E). The trend for correlation to decrease with increased marine influence (e.g. tidal, wave or backwater-controlled flow regimes) is anticipated, and existing hydraulic geometry models assume unidirectional river flow (Gleason and Smith, 2014). However, in wave–dominated systems the wave energy appears to have minimal impact on channel widths, and thus significant width-discharge scaling relationships can be obtained (Fig. 6E).

Reconstructing water discharge of an ancient fluvial and/or delta system relies on accurate measurement of channel geometry from channel fills (Parker et al., 2007; Hayden et al., 2019). In outcrop or subsurface datasets, it is commonly easier to measure distributary channel depths than widths. However, satellite imageries that we used in this study limit our observation of distributary channel depths. If width-depth empirical relationships from modern river deltas exist, transformation from our width-discharge to depth-discharge could be scaled accordingly by assuming a steady flow and equilibrium depth and slope. Moreoever, several issues influence the accuracy of width measurements from outcrops. The measured channel fill may not be perpendicular to the paleoflow (Holbrook and Wanas, 2014; Bhattacharya et al., 2016) and infill deposits are often incompletely preserved (Bridge and Mackey, 1993; Bridge and Tye, 2000). When the channel fill deposit is incomplete, width-depth scaling relationships can still be used, albeit they contain substantial uncertainty because channel fill dimensions can differ significantly from formative channel dimensions (Hayden et al., 2019; Greenberg et al., 2021).

The proposed scaling relationships should not be used as a standalone model to interpret the paleodischarge from the rock record. Uncertainties exist in both the field data and the statistical relationships; hence, the results provide discharge ranges based on the propagation of these uncertainties. Additional information should be gathered from outcrops to further constrain the predicted paleodischarge; this may include stratigraphic context, sedimentary structures, grain size, fossil assemblages and vegetation amongst others. As an example, using the scaling relationship for the upstream part of river-dominated deltas (Fig. 6A), a median distributary channel width of 300 m gives a discharge range of Q_2 = 3077±12 m^3/s (i.e. ± is from the error propagation produced by regression and distributary channel width of the upstream part of river-dominated deltas). The uncertainty in paleodischarge values is considerably greater in marine-influenced deltas, namely the downstream part of river-dominated deltas or wave-dominated deltas. Thus, the interpretation of paleodischarge requires contextual information that may support or challenge the calculated values.

In order to assess paleodischarge estimated using our approach, we utilize the case study from the lower Mesa Rica. The plain of the lower Mesa Rica delta is approximately 100 km long, measured in river kilometres from the shoreline to the most landward avulsion node (Fig. 3). In terms of delta plain size, the lower Mesa Rica is comparable with the modern Brahmani (1800 km^2) and Mahanadi (1700 km^2) deltas, although in terms of average bankfull channel depth (Table S1), the smaller Danube (5800 km^2), Ebro (460 km^2) and Mahanadi are better comparisons. The discharge of the lower Mesa Rica is more comparable to total system discharge coming into Ebro, Cauvery, Wax Lake, Sanaga and Rio Sinú deltas (GRDC; Bhattacharya and Tye, 2004). These comparisons indicate that the lower Mesa Rica is comparable with many modern deltas but none of them provides a perfect fit in terms of geometry (delta area, bankfull channel depth) and in input discharge. The number and diversity of potential modern delta analogues for the Mesa Rica

Formation illustrates how scaling relationships from modern systems should not be used in isolation.

The difference in widths in river-dominated deltas between their upstream and downstream parts leads to differences in the statistical significance and uncertainty associated with scaling relationships for the two parts. Consequently, the number of measurements required to estimate input discharge to a specified level of uncertainty varies with the location of measurements along the delta. In some well-studied systems this specification of location is possible, potentially alongside information on climate type, and thus the methods shown in this study are applicable. Where context is unknown the scaling relationships provided here should be used with caution.

CONCLUSION

Distinct down-dip patterns of dimensionless distributary channel widths are recognized from measurements from 114 modern global river deltas. River- and tide-dominated deltas show significant channel widening at s/L = 0.05 (i.e. near shoreline) and 0.45 (i.e. approximately halfway across the delta plain from the shoreline to the apex), respectively. Mouth bar depositional cycles in river-dominated deltas and tidal energy obstructing unidirectionality of channel currents in tide-dominated deltas are the main cause of these distinct patterns. In contrast, wave-dominated deltas show consistent dimensionless distributary channel width down-dip. Calculation of paleodischarge is based on empirical relationships between median channel width and input river discharge. By bootstrapping the dimensionless distributary channel widths from modern deltas, this study provides estimates of the minimum number of measurements required to estimate median width to a specified standard error. We calculate the minimum number of measurements required to reduce the standard error of dimensionless width to 0.5 as follows (in parentheses): upstream (3) and downstream (30) parts of river-dominated deltas; upstream part of tide-dominated deltas (6);

and, wave-dominated deltas (4). The downstream part of tide-dominated deltas produces very high standard error (>1.5) with any number of samples and input discharge cannot be reliably estimated from channels in these locations. Applying the proposed distributary channel width-discharge scaling relationships from modern deltas to the well-studied lower Mesa Rica formation produced a comparable paleodischarge estimate to that from the Fulcrum method. The results from this study improve paleoclimate and tectonic reconstruction, volumetric assessment of hydrocarbon, hydrogen and geothermal reservoirs, in diverse depositional environments. Second, the results enable more detailed paleohydraulics reconstruction across various types of depositional systems in source-to-sink investigations.

ACKNOWLEDGMENTS

We thank Ivar Midtkandal (University of Oslo) who initiated collaboration between Anna van Yperen and the University of Glasgow. The research was funded by The Indonesia Endowment Fund for Education (LPDP) awarded to Prasojo.

DATA AVAILABILITY STATEMENT

Data from this paper (Table S2) are available in the open repository (https://doi.org/10.6084/m9.figshare.19964549.v2). The global river discharge data set is available from The Global Runoff Data Centre (GRDC), 56068 Koblenz, Germany and via the web (https://www.bafg.de/GRDC/EN/02_srvcs/21_tmsrs/210_prtl/prtl_node.html).

REFERENCES

Allen, G. H., and Pavelsky, T. M., 2018, Global extent of rivers and streams: Science, v. 361, p. 585–588.

Allen, G. P., Salomon, J. C., Bassoullet, P., Du Penhoat, Y., and de Grandpré, C., 1980, Effects of tides on mixing and suspended sediment transport in macrotidal estuaries: Sedimentary Geology, v. 26, p. 69–90.

Allen, P. A., Armitage, J. J., Carter, A., Duller, R. A., Michael, N. A., Sinclair, H. D., Whitchurch, A. L., and Whittaker, A. C., 2013, The Qs problem: Sediment volumetric balance of proximal foreland basin systems: Sedimentology, v. 60, p. 102–130.

Beck, H. E., Zimmermann, N. E., McVicar, T. R., Vergopolan, N., Berg, A., and Wood, E. F., 2018, Present and future köppen-geiger climate classification maps at 1-km resolution: Scientific Data, v. 5, p. 1–12.

van den Berg, J. H., Boersma, J. R., and van Gelder, A., 2007, Diagnostic sedimentary structures of the fluvial-tidal transition zone - Evidence from deposits of the Rhine and Meuse: Geologie en Mijnbouw/Netherlands Journal of Geosciences, v. 86, p. 287–306.

Besset, M., Anthony, E. J., and Sabatier, F., 2017, River delta shoreline reworking and erosion in the Mediterranean and Black Seas: the potential roles of fluvial sediment starvation and other factors: Elem Sci Anth, v. 5, p. 54.

Bhatt, V. K., and Tiwari, A. K., 2008, Estimation of peak streamflows through channel geometry / Estimation de pics de débit fluviatiles à l’aide de la géométrie des cours d’eau Estimation of peak streamflows through channel geometry: Hydrological Sciences-Journal-des Sciences Hydrologiques, v. 53, p. 401–408.

Bhattacharya, J. P., and Giosan, L., 2003, Wave-influenced deltas: Geomorphological implications for facies reconstruction: Sedimentology, v. 50, p. 187–210.

Bhattacharya, J. P., and Tye, R. S., 2004, Searching for modern Ferron analogs and application to subsurface interpretation, in Chidsey, T. C., Adams, R. D., and Morris, T. H. eds., Regional to Wellbore Analog for Fluvial–Deltaic Reservoir Modeling: the Ferron Sandstone of Utah: American Association of Petroleum Geologists, Studies in Geology 50: American Association of Petroleum Geologists, p. 39–57.

Bhattacharya, J. P., Copeland, P., Lawton, T. F., and Holbrook, J., 2016, Estimation of source area, river paleo-discharge, paleoslope, and sediment budgets of linked deep-time depositional systems and implications for hydrocarbon potential: Earth-Science Reviews, v. 153, p. 77–110.

Brardinoni, F., and Hassan, M. A., 2006, Glacial erosion, evolution of river long profiles, and the organization of process domains in mountain drainage basins of coastal British Columbia: Journal of Geophysical Research, v. 111, p. F01013.

Brewer, C. J., Hampson, G. J., Whittaker, A. C., Roberts, G. G., and Watkins, S. E., 2020, Comparison of methods to estimate sediment flux in ancient sediment routing systems: Earth-Science Reviews, v. 207, p. 103217.

Bridge, J. S., and Mackey, S. D., 1993, A theoretical study of fluvial sandstone body dimensions, in The Geological Modelling of Hydrocarbon Reservoirs and Outcrop Analogues: wiley, p. 213–236.

Bridge, J. S., and Tye, R. S., 2000, Interpreting the Dimensions of Ancient Fluvial Channel Bars, Channels, and Channel Belts from Wireline-Logs and Cores: AAPG Bulletin, v. 84, p. 1205–1228.

Caldwell, R. L., Edmonds, D. A., Baumgardner, S., Paola, C., Roy, S., and Nienhuis, J. H., 2019, A global delta dataset and the environmental variables that predict delta formation on marine coastlines: Earth Surface Dynamics, v. 7, p. 773–787.

Castelltort, S., Goren, L., Willett, S. D., Champagnac, J. D., Herman, F., and Braun, J., 2012, River drainage patterns in the New Zealand Alps primarily controlled by plate tectonic strain: Nature Geoscience, v. 5, p. 744–748.

Chadwick, A. J., Lamb, M. P., Moodie, A. J., Parker, G., and Nittrouer, J. A., 2019, Origin of a Preferential Avulsion Node on Lowland River Deltas: Geophysical Research Letters, v. 46, p. 4267–4277.

Chadwick, A. J., Lamb, M. P., and Ganti, V., 2020, Accelerated river avulsion frequency on lowland deltas due to sea-level rise: Proceedings of the National Academy of Sciences of the United States of America, v. 117, p. 17584–17590.

Chatanantavet, P., Lamb, M. P., and Nittrouer, J. A., 2012, Backwater controls of avulsion location on deltas: Geophysical Research Letters, v. 39, p. 2–7.

Cheng, A., and Yeager, M., 2007, Bootstrap resampling for voxel-wise variance analysis of three-dimensional density maps derived by image analysis of two-dimensional crystals: Journal of Structural Biology, v. 158, p. 19–32.

Chumakov, N., Zharkov, M. A., Herman, A. B., Doludenko, M. P., Kalandadze, N. N., Lebedev, E. L., Ponomarenko, A. G., and Rautian, A. S., 1995, Climatic Belts of the Mid-Cretaceous Time: Stratigraphy and Geological Correlation, v. 3, p. 42–63.

Cohen, S., Kettner, A. J., Syvitski, J. P. M., and Fekete, B. M., 2013, WBMsed, a distributed global-scale riverine sediment flux model: Model description and validation: Computers and Geosciences, v. 53, p. 80–93.

Colombera, L., Mountney, N. P., Medici, G., and West, L. J., 2019, The geometry of fluvial channel bodies: Empirical characterization and implications for object-based models of the subsurface: AAPG Bulletin, v. 103, p. 905–929.

Cui, M., Xu, L., Wang, H., Ju, S., Xu, S., and Jing, R., 2017, Combining Nordtest method and bootstrap resampling for measurement uncertainty estimation of hematology analytes in a medical laboratory: Clinical Biochemistry, v. 50, p. 1067–1072.

Dalrymple, R. W., and Choi, K., 2007, Morphologic and facies trends through the fluvial-marine transition in tide-dominated depositional systems: A schematic framework for environmental and sequence-stratigraphic interpretation: Earth-Science Reviews, v. 81, p. 135–174.

Dalrymple, R. W., Kurcinka, C. E., Jablonski, B. V. J., Ichaso, A. A., and Mackay, D. A., 2015, Deciphering the relative importance of fluvial and tidal processes in the fluvial-marine transition, in Developments in Sedimentology: Elsevier, p. 3–45.

Dashtgard, S. E., Venditti, J. G., Hill, P. R., Sisulak, C. F., Johnson, S. M., and Croix, A. D. La, 2012, Sedimentation Across the Tidal-Fluvial Transition in the Lower Fraser River, Canada: The Sedimentary Record.

Davidson, S. K., and Hartley, A. J., 2010, Towards a quantitative method for estimating paleohydrology from clast size and comparison with modern rivers: Journal of Sedimentary Research, v. 80, p. 688–702.

Davidson, S. K., and North, C. P., 2009, Geomorphological regional curves for prediction of drainage area and screening modern analogues for rivers in the rock record: Journal of Sedimentary Research, v. 79, p. 773–792.

Debchoudhury, S., Sengupta, S., Earle, G., and Coley, W., 2019, A Bootstrap-Based Approach for Improving Measurements by Retarding Potential Analyzers: Journal of Geophysical Research: Space Physics, v. 124, p. 4569–4584.

Diefenderfer, H. L., Coleman, A. M., Borde, A. B., and Sinks, I. A., 2008, Hydraulic geometry and microtopography of tidal freshwater forested wetlands and implications for restoration, Columbia River, U.S.A.: Ecohydrology and Hydrobiology, v. 8, p. 339–361.

Duller, R. A., Whittaker, A. C., Fedele, J. J., Whitchurch, A. L., Springett, J., Smithells, R., Fordyce, S., and Allen, P. A., 2010, From grain size to tectonics: Journal of Geophysical Research: Earth Surface, v. 115, p. 3022.

Dunne, K. B. J., and Jerolmack, D. J., 2020, What sets river width? Science Advances, v. 6, p. eabc1505.

Eaton, B. C., 2013, Hydraulic Geometry: Empirical Investigations and Theoretical Approaches, in Treatise on Geomorphology: Elsevier Inc., p. 313–329.

Edmonds, D. A., and Slingerland, R. L., 2007, Mechanics of river mouth bar formation: Implications for the morphodynamics of delta distributary networks: Journal of Geophysical Research: Earth Surface, v. 112.

Efron, B., 1982, The Jackknife, the Bootstrap and Other Resampling Plans: Society for Industrial and Applied Mathematics.

Efron, B., 2007, Bootstrap Methods: Another Look at the Jackknife: The Annals of Statistics, v. 7, p. 1–26.

Eide, C. H., Müller, R., and Helland-Hansen, W., 2018, Using climate to relate water discharge and area in modern and ancient catchments (V. Manville, Ed.): Sedimentology, v. 65, p. 1378–1389.

Fernandes, A. M., Törnqvist, T. E., Straub, K. M., and Mohrig, D., 2016, Connecting the backwater hydraulics of coastal rivers to fluviodeltaic sedimentology and stratigraphy: Geology, v. 44, p. 979–982.

Frasson, R. P. de M., Pavelsky, T. M., Fonstad, M. A., Durand, M. T., Allen, G. H., Schumann, G., Lion, C., Beighley, R. E., and Yang, X., 2019, Global Relationships Between River Width, Slope, Catchment Area, Meander Wavelength, Sinuosity, and Discharge: Geophysical Research Letters, v. 46, p. 3252–3262.

Galloway, W. D., 1975, Process Framework for describing the morphologic and stratigraphic evolution of deltaic depositional systems: Houston Geological Society. Deltas: Models for Exploration, p. 87–98.

Ganti, V., Chadwick, A. J., Hassenruck-Gudipati, H. J., Fuller, B. M., and Lamb, M. P., 2016, Experimental river delta size set by multiple floods and backwater hydrodynamics: Science Advances, v. 2, p. e1501768.

Gisen, J. I. A., and Savenije, H. H. G., 2015, Estimating bankfull discharge and depth in ungauged estuaries: Water Resources Research, v. 51, p. 2298–2316.

Gleason, C. J., 2015, Hydraulic geometry of natural rivers: A review and future directions: Progress in Physical Geography, v. 39, p. 337–360.

Gleason, C. J., Wada, Y., and Wang, J., 2018, A Hybrid of Optical Remote Sensing and Hydrological Modeling Improves Water Balance Estimation: Journal of Advances in Modeling Earth Systems, v. 10, p. 2–17.

Greenberg, E., Ganti, V., and Hajek, E., 2021, Quantifying bankfull flow width using preserved bar clinoforms from fluvial strata: Geology, v. 1.

Gugliotta, M., and Saito, Y., 2019, Matching trends in channel width, sinuosity, and depth along the fluvial to marine transition zone of tide-dominated river deltas: The need for a revision of depositional and hydraulic models: Earth-Science Reviews, v. 191, p. 93–113.

Gugliotta, M., Flint, S. S., Hodgson, D. M., and Veiga, G. D., 2016, Recognition criteria, characteristics and implications of the fluvial to marine transition zone in ancient deltaic deposits (Lajas Formation, Argentina): Sedimentology, v. 63, p. 1971–2001.

Gugliotta, M., Saito, Y., Nguyen, V. L., Ta, T. K. O., and Tamura, T., 2019, Sediment distribution and depositional processes along the fluvial to marine transition zone of the Mekong River delta, Vietnam: Sedimentology, v. 66, p. 146–164.

Hampson, G. J., Jewell, T. O., Irfan, N., Gani, M. R., and Bracken, B., 2013, Modest change in fluvial style with varying accommodation in regressive alluvial-to-coastal-plain wedge: Upper Cretaceous Blackhawk Formation, Wasatch Plateau, central Utah, U.S.A: Journal of Sedimentary Research, v. 83, p. 145–169.

Hartley, A. J., Weissmann, G. S., and Scuderi, L., 2017, Controls on the apex location of large deltas: Journal of the Geological Society, v. 174, p. 10–13.

Haucke, J., and Clancy, K. A., 2011, Stationarity of streamflow records and their influence on bankfull regional curves: Journal of the American Water Resources Association, v. 47, p. 1338–1347.

Hayden, A. T., Lamb, M. P., Fischer, W. W., Ewing, R. C., McElroy, B. J., and Williams, R. M. E., 2019, Formation of sinuous ridges by inversion of river-channel belts in Utah, USA, with implications for Mars: Icarus, v. 332, p. 92–110.

Holbrook, J., 2001, Origin, genetic interrelationships, and stratigraphy over the continuum of fluvial channel-form bounding surfaces: An illustration from middle Cretaceous strata, Southeastern Colorado: Sedimentary Geology, v. 144, p. 179–222.

Holbrook, J., and Wanas, H., 2014, A fulcrum approach to assessing source-to-sink mass balance using channel paleohydrologic paramaters derivable from common fluvial data sets with an example from the cretaceous of Egypt: Journal of Sedimentary Research, v. 84, p. 349–372.

Holbrook, J. M., 1996, Complex fluvial response to low gradients at maximum regression: A genetic link between smooth sequence-boundary morphology and architecture of overlying sheet sandstone: Journal of Sedimentary Research, v. 66, p. 713–722.

Jablonski, B. V. J., and Dalrymple, R. W., 2016, Recognition of strong seasonality and climatic cyclicity in an ancient, fluvially dominated, tidally influenced point bar: Middle McMurray Formation, Lower Steepbank River, north-eastern Alberta, Canada: Sedimentology, v. 63, p. 552–585.

Jacobsen, R. E., and Burr, D. M., 2016, Greater contrast in Martian hydrological history from more accurate estimates of paleodischarge: Geophysical Research Letters, v. 43, p. 8903–8911.

Kästner, K., Hoitink, A. J. F., Vermeulen, B., Geertsema, T. J., and Ningsih, N. S., 2017, Distributary channels in the fluvial to tidal transition zone: Journal of Geophysical Research: Earth Surface, v. 122, p. 696–710.

Korus, J. T., and Fielding, C. R., 2015, Asymmetry in Holocene river deltas: Patterns, controls, and stratigraphic effects: Earth-Science Reviews, v. 150, p. 219–242.

Kravtsova, V. I., Mikhailov, V. N., and Kidyaeva, V. M., 2009, Hydrological regime, morphological features and natural territorial complexes of the Irrawaddy River Delta (Myanmar): Water Resources, v. 36, p. 243–260.

Lamb, M. P., Nittrouer, J. A., Mohrig, D., and Shaw, J., 2012, Backwater and river plume controls on scour upstream of river mouths: Implications for fluvio-deltaic morphodynamics: J. Geophys. Res, v. 117, p. 1002.

Leclair, S. F., and Bridge, J. S., 2001, Quantitative interpretation of sedimentary structures formed by river dunes: Journal of Sedimentary Research, v. 71, p. 713–716.

Leopold, L. B., and Maddock, T., 1953, The Hydraulic Geometry of Stream Channels and Some Physiographic Implications:, accessed at Professional Paper.

Li, W., Bhattacharya, J. P., and Wang, Y., 2011, Delta asymmetry: Concepts, characteristics, and depositional models: Petroleum Science, v. 8, p. 278–289.

Lin, W., and Bhattacharya, J. P., 2017, Estimation of source-to-sink mass balance by a fulcrum approach using channel paleohydrologic parameters of the cretaceous dunvegan formation, Canada: Journal of Sedimentary Research, v. 87, p. 97–116.

Lin, W., and Bhattacharya, J. P., 2021, Storm-flood-dominated delta: A new type of delta in stormy oceans: Sedimentology, v. 68, p. 1109–1136.

Lyster, S. J., Whittaker, A. C., Allison, P. A., Lunt, D. J., and Farnsworth, A., 2020, Predicting sediment discharges and erosion rates in deep time—examples from the late Cretaceous North American continent: Basin Research, v. 32, p. 1547–1573.

Lyster, S. J., Whittaker, A. C., Hampson, G. J., Hajek, E. A., Allison, P. A., and Lathrop, B. A., 2021, Reconstructing the morphologies and hydrodynamics of ancient rivers from source to sink: Cretaceous Western Interior Basin, Utah, USA: Sedimentology.

Martin, J., Fernandes, A. M., Pickering, J., Howes, N., Mann, S., and McNeil, K., 2018, The Stratigraphically Preserved Signature of Persistent Backwater Dynamics in a Large Paleodelta System: The Mungaroo Formation, North West Shelf, Australia: Journal of Sedimentary Research, v. 88, p. 850–872.

Merritt, D. M., and Wohl, E. E., 2003, Downstream hydraulic geometry and channel adjustment during a flood along an ephemeral, arid-region drainage: Geomorphology, v. 52, p. 165–180.

Montgomery, D. R., and Gran, K. B., 2001, Downstream variations in the width of bedrock channels: Water Resources Research, v. 37, p. 1841–1846.

Morgan, A. M., and Craddock, R. A., 2019, Assessing the Accuracy of Paleodischarge Estimates for Rivers on Mars: Geophysical Research Letters, v. 46, p. 11738–11746.

Nienhuis, J. H., Ashton, A. D., Edmonds, D. A., Hoitink, A. J. F., Kettner, A. J., Rowland, J. C., and Törnqvist, T. E., 2020, Global-scale human impact on delta morphology has led to net land area gain: Nature, v. 577, p. 514–518.

Nittrouer, J. A., 2013, Backwater hydrodynamics and sediment transport in the lowermost Mississippi River delta: Implications for the development of fluvial-deltaic landforms in a large lowland river, in IAHS ed., Proceedings of HP1, IAHS-IAPSO-IASPEI Assembly, Gothenburg, Sweden, July 2013 (IAHS Publ. 358, 2013).: Gothenburg, IAHS Publication.

Nyberg, B., Helland-Hansen, W., Gawthorpe, R., Tillmans, F., and Sandbakken, P., 2021, Assessing First-Order BQART Estimates for Ancient Source-to-Sink Mass Budget Calculations: Basin Research, v. 00, p. 1–18.

Oboh-Ikuenobe, F., Holbrook, J., Scott, R., Akins, S., Evetts, M., Benson, D., and Pratt, L., 2008, Anatomy of Epicontinental Flooding: Late Albian-Early Cenomanian of the Southern U.S. Western Interior Basin: Special Paper - Geological Association of Canada.

Olariu, C., and Bhattacharya, J. P., 2006, Terminal distributary channels and delta front architecture of river-dominated delta systems: Journal of Sedimentary Research, v. 76, p. 212–233.

Parker, G., Wilcock, P. R., Paola, C., Dietrich, W. E., and Pitlick, J., 2007, Physical basis for quasi-universal relations describing bankfull hydraulic geometry of single-thread gravel bed rivers: Journal of Geophysical Research: Earth Surface, v. 112.

De Rose, R. C., Stewardson, M. J., and Harman, C., 2008, Downstream hydraulic geometry of rivers in Victoria, Australia: Geomorphology, v. 99, p. 302–316.

R.W. Scott, J.M. Holobrook, F.E. Oboh-Ikuenobe, M.J. Evetts, D.G. Benson, and B.S. Kues, 2004, Middle Cretaceous Stratigraphy, Southern Western Interior Seaway, New Mexico and Oklahoma: The Mountain Geologist.

Sassi, M. G., Hoitink, A. J. F., de Brye, B., and Deleersnijder, E., 2012, Downstream hydraulic geometry of a tidally influenced river delta: Journal of Geophysical Research: Earth Surface, v. 117, p. n/a-n/a.

Sharma, S., Bhattacharya, J. P., and Richards, B., 2017, Source-to-sink sediment budget analysis of the Cretaceous Ferron Sandstone, Utah, U.S.A, using the fulcrum approach: Journal of Sedimentary Research, v. 87, p. 594–608.

Sharman, G. R., Sylvester, Z., and Covault, J. A., 2019, Conversion of tectonic and climatic forcings into records of sediment supply and provenance: Scientific Reports 2019 9:1, v. 9, p. 1–7.

Swenson, J. B., 2005, Relative importance of fluvial input and wave energy in controlling the timescale for distributary-channel avulsion: Geophysical Research Letters, v. 32, p. 1–5.

Syvitski, J. P. M., and Milliman, J. D., 2007, Geology, Geography, and Humans Battle for Dominance over the Delivery of Fluvial Sediment to the Coastal Ocean: The Journal of Geology, v. 115, p. 1–19.

Trampush, S. M., Huzurbazar, S., and McElroy, B., 2014, Empirical assessment of theory for bankfull characteristics of alluvial channels: Water Resources Research, v. 50, p. 9211–9220.

Vakarelov, B. K., and Ainsworth, R. B., 2013, A hierarchical approach to architectural classification in marginal-marine systems: Bridging the gap between sedimentology and sequence stratigraphy: AAPG Bulletin, v. 97, p. 1121–1161.

Whittaker, A. C., 2012, How do landscapes record tectonics and climate? Lithosphere, v. 4, p. 160–164.

Whittaker, A. C., Duller, R. A., Springett, J., Smithells, R. A., Whitchurch, A. L., and Allen, P. A., 2011, Decoding downstream trends in stratigraphic grain size as a function of tectonic subsidence and sediment supply: Bulletin of the Geological Society of America, v. 123, p. 1363–1382.

Wohl, E., and David, G. C. L., 2008, Consistency of scaling relations among bedrock and alluvial channels: Journal of Geophysical Research, v. 113, p. F04013.

van Yperen, A. E., Holbrook, J. M., Poyatos-Moré, M., and Midtkandal, I., 2019, Coalesced delta-front sheet-like sandstone bodies from highly avulsive distributary channels: The low-accommodation mesa rica sandstone (Dakota Group, New Mexico, USA): Journal of Sedimentary Research, v. 89, p. 654–678.

van Yperen, A. E., Holbrook, J. M., Poyatos-Moré, M., Myers, C., and Midtkandal, I., 2020, Low-accommodation and backwater effects on sequence stratigraphic surfaces and depositional architecture of fluvio-deltaic settings (Cretaceous Mesa Rica Sandstone, Dakota Group, USA): Basin Research, v. 33, p. 513–543.

FIGURE CAPTIONS

Figure 1. Landsat 5 images (all around year 2000) from: A. tide-influenced, river-dominated Mahakam delta, Indonesia; B. wave-influenced Baram delta, Malaysia; tide-dominated C. tide-

dominated Fly delta, Papua New Guinea and D. river-dominated Pahang delta, Malaysia. Changes in channel width away from the distal limits, which are plotted in the lower panels. Differences in morphological patterns depend on the interaction between dynamic catchment (water and sediment inputs) and marine (wave energy, tidal energy) variables that interact to produce delta morphology.

Figure 2. A: The semicircular grid used to measure the channel widths of distributary channels. B: Enlarged version of the measured channel width from Fig. 2A. Channel widths were made at the red lines which are perpendicular to the banks of the wetted distributary channels. Inset shows measurement method when mid-channel bars are present. The spacing of the semicircular grid is defined as ~10 times the channel width at the apex of the delta (W_A).

Figure 3. Paleogeographic reconstruction of the Cretaceous lower Mesa Rica fluvio-deltaic depositional system (modified from Van Yperen et al., 2019). Nevertheless, due to the scale of the figure, not all 13 data points could be drawn on the figure. See Table 1 for the exact location of all channel width measurements.

Figure 4. A-C: Distribution of dimensionless measured channel widths from (A) river-, (B) tide- and, (C) wave-dominated deltas. *p*-values are from the non-parametric Kruskal-Wallis one-way analysis of variance test comparing the distributions of channel width at different locations along the delta. D-E: examples of (D) river- and (E) tide-dominated deltas, with the upstream-downstream boundary positions inferred from the changes of channel width on (A) and (B). F: Map view the Paraibo do Sul delta in Brazil showing differences in ‘updrift’ and ‘downdrift’

characteristics of a wave-dominated delta (modified from Li et al., 2011). G: Map view and cross-section view of a mouth bar. Boxes on D depict the location of the mouth bars shown in G.

Figure 5. Mean standard error of dimensionless channel width (S_{W*}) versus number of measurements (N) from the upstream and downstream parts of river- (A,B, respectively) and tide-dominated (C,D) deltas. E: Mean standard error versus N from wave-dominated deltas. F-K: Percentile standard errors of the dimensionless widths for the selected B values from plots (A-E). B indicates the number of repetitions in the bootstrap calculations. Inset plots (A-E) show greater detail for low N. The dark orange lines show the number of repetitions (B) that produced the most stable, generally monotonic relationships between standard error of dimensionless width and number of measurements.

Figure 6. A-E: Scaling relationships between bankfull discharge (Q_2) and median channel widths (W_{med}) for river-, tide-, wave-dominated deltas. (F) Scaling relationship between bankfull discharge (Q_2) and channel widths (W) for overall dataset. (A) and (C) are for upstream parts of river- and/ tide-dominated deltas, and (B) and (D) are for their downstream parts, respectively Ordinary least squares regression lines and 95% confidence intervals (shaded areas) shown; R^2 = coefficient of determination of the scaling relationship, p = statistical significance, and s = standard error of residuals.

Figure 7. A: Distribution of 13 measured channel widths from the lower Mesa Rica, grouped by geographical zone across the delta plain. B: Density plot of the 13 measured channel widths: whole population (dark yellow); transitional zone (grey); and, distal zone (dark blue). Median,

mean, and mode values (continuous, dashed and dotted vertical lines, respectively) are calculated from the combined transitional and distal data (N=12), excluding the single width measurement from the proximal zone. C: Standard error of dimensionless width (S_{W*}) versus number of samples (N) of the 12 measured channel widths from the lower Mesa Rica.

TABLE CAPTIONS

Table 1. Distribution of the 13 measured channel widths from the lower Mesa Rica along with the zonation and latitude-longitude positions.

Figure 1

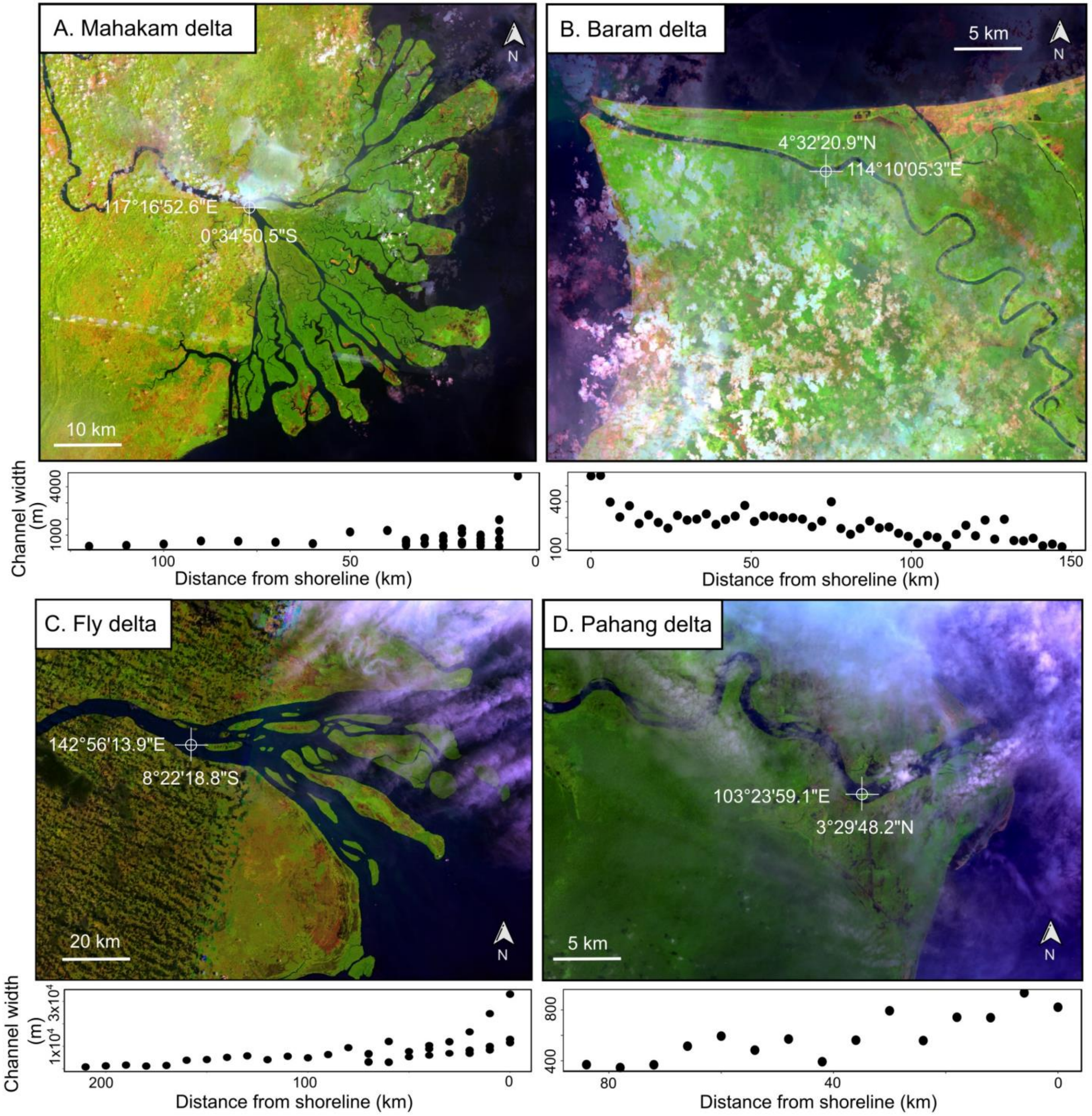

A. Mahakam delta
117°16'52.6"E
0°34'50.5"S
10 km
N
B. Baram delta
5 km
N
4°32'20.9"N
114°10'05.3"E
C. Fly delta
142°56'13.9"E
8°22'18.8"S
20 km
N
D. Pahang delta
103°23'59.1"E
3°29'48.2"N
5 km
N
Channel width (m)
Distance from shoreline (km)

Figure 2

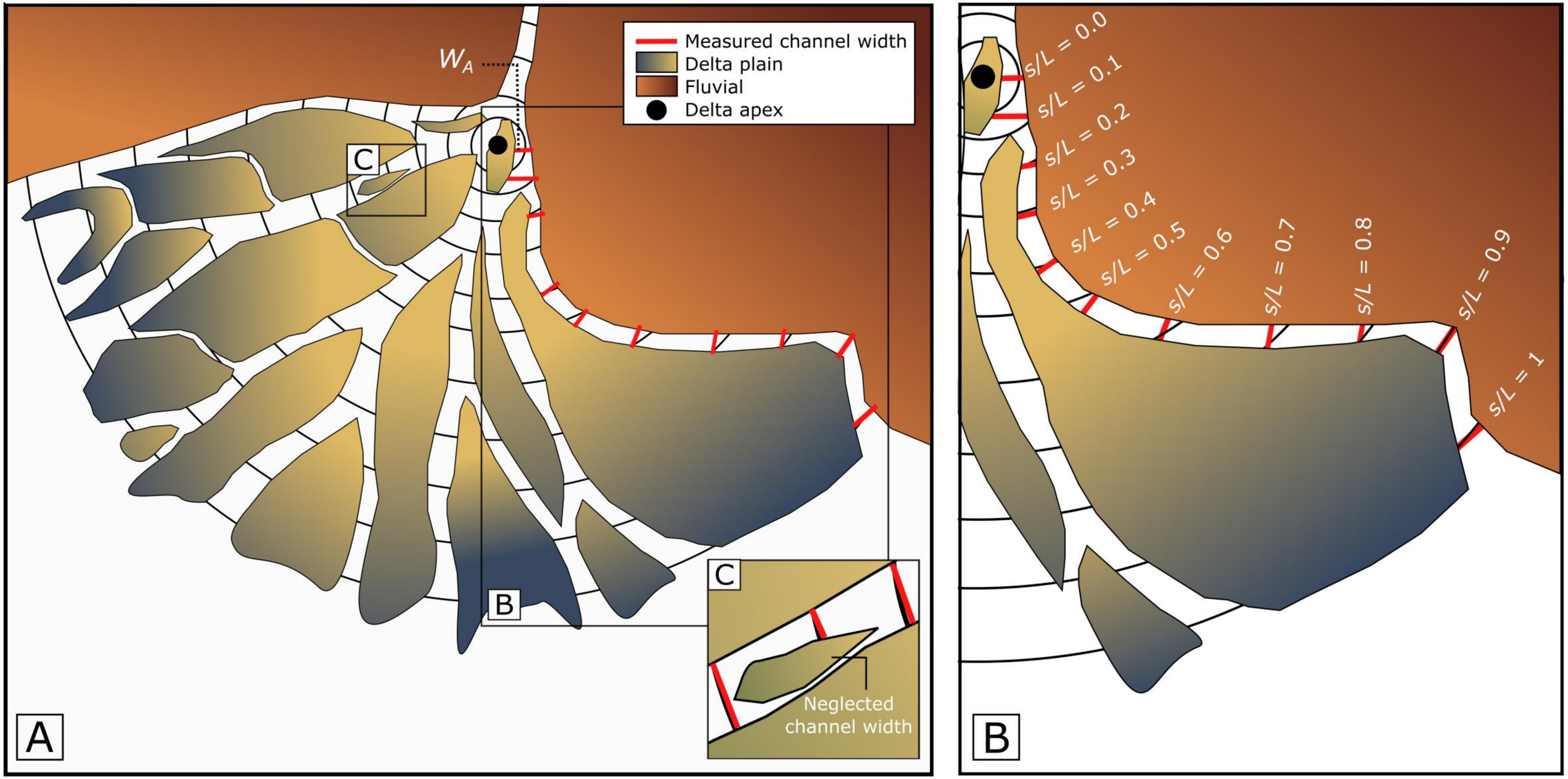

Measured channel width
Delta plain
Fluvial
Delta apex
W_A
C
B
C
Neglected channel width
A
s/L = 0.0
s/L = 0.1
s/L = 0.2
s/L = 0.3
s/L = 0.4
s/L = 0.5
s/L = 0.6
s/L = 0.7
s/L = 0.8
s/L = 0.9
s/L = 1
B

Figure 3

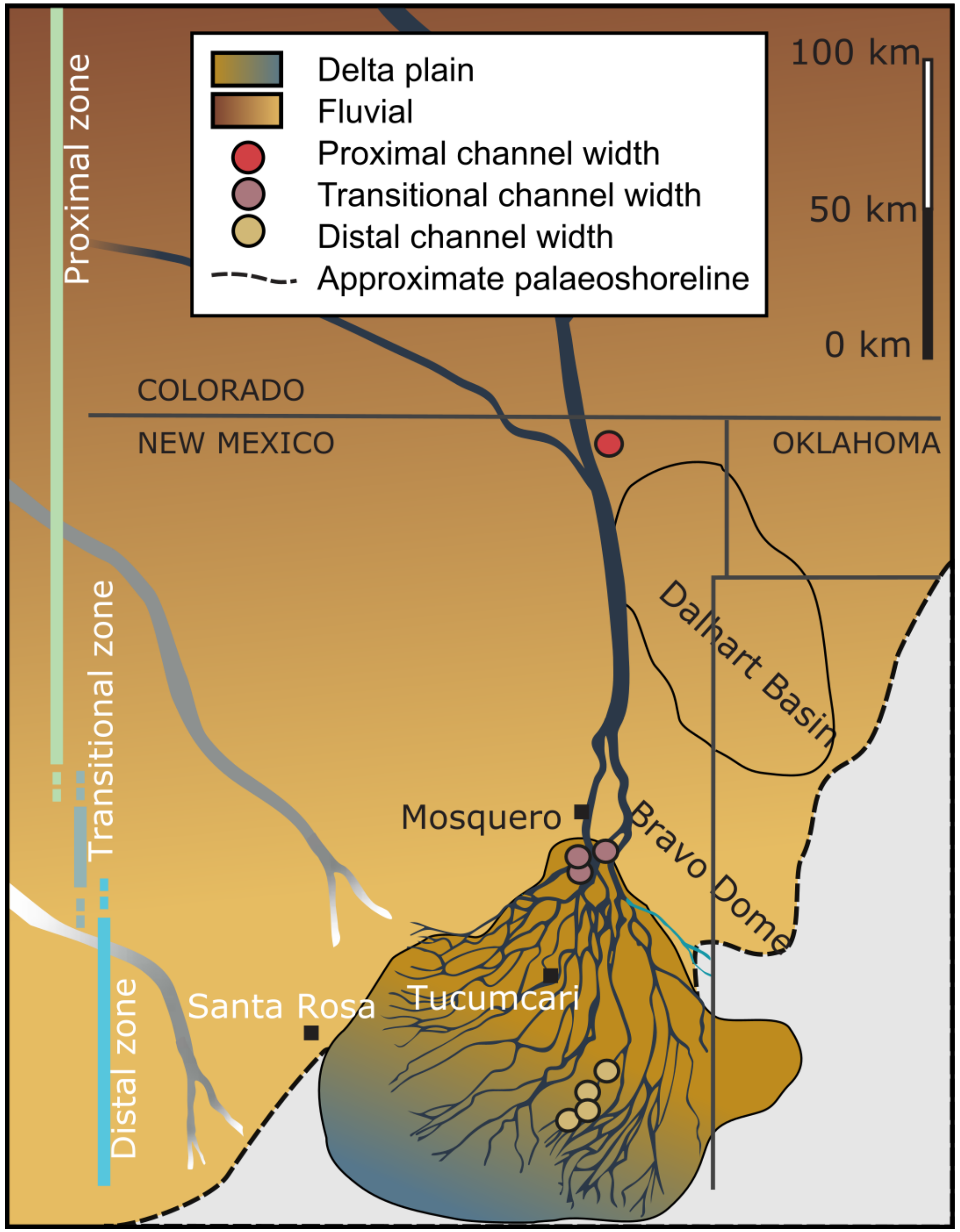

Delta plain
Fluvial
Proximal channel width
Transitional channel width
Distal channel width
Approximate palaeoshoreline
100 km
50 km
0 km
Proximal zone
Transitional zone
Distal zone
COLORADO
NEW MEXICO
OKLAHOMA
Dalhart Basin
Bravo Dome
Mosquero
Santa Rosa
Tucumcari

Figure 4

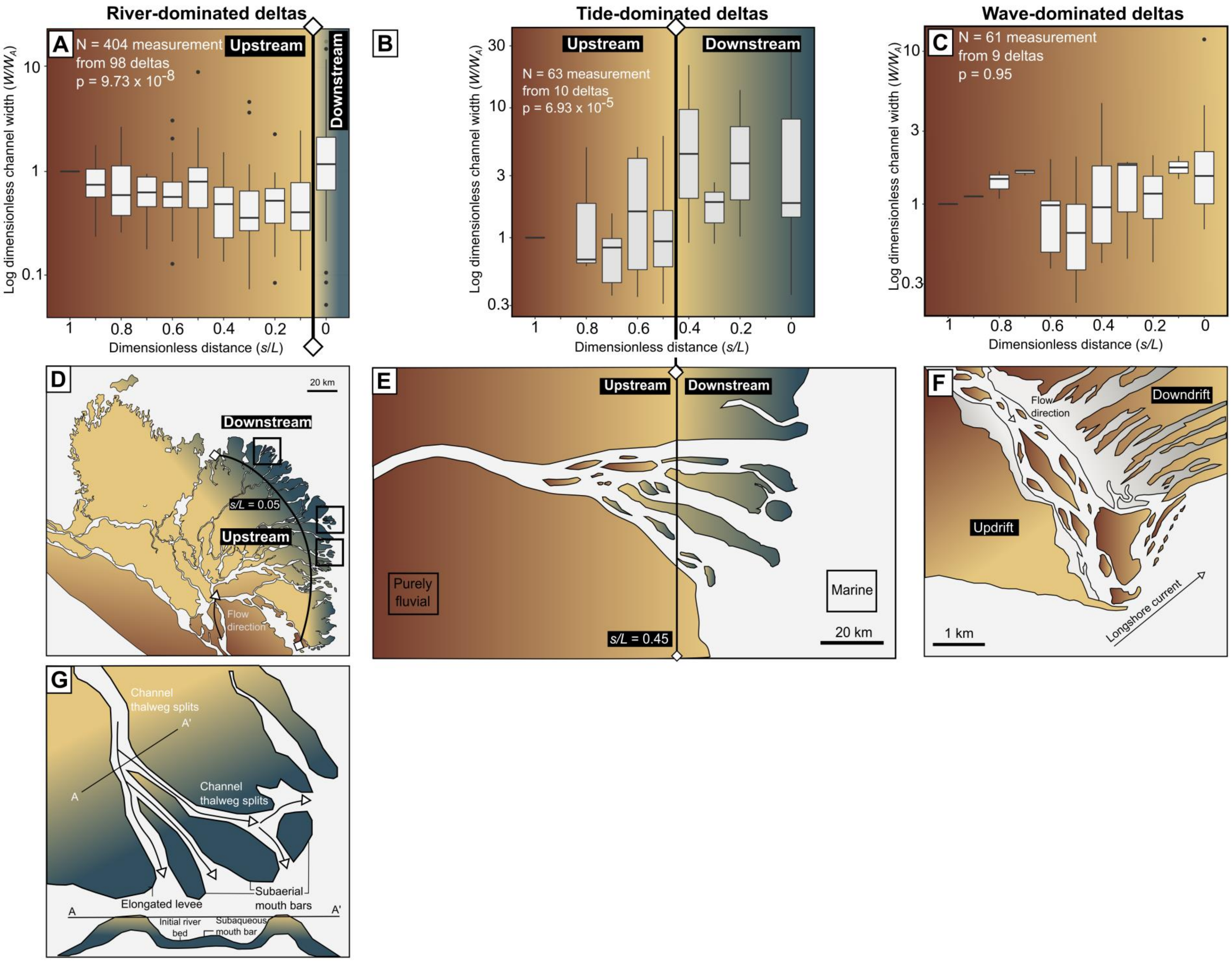

River-dominated deltas
Tide-dominated deltas
Wave-dominated deltas
A
N = 404 measurement
from 98 deltas
p = 9.73 x 10^-8
Upstream
Downstream
Log dimensionless channel width (W/W_A)
Dimensionless distance (s/L)
B
Upstream
Downstream
N = 63 measurement
from 10 deltas
p = 6.93 x 10^-5
C
N = 61 measurement
from 9 deltas
p = 0.95
D
20 km
Downstream
s/L = 0.05
Upstream
Flow
direction
E
Upstream
Downstream
Purely
fluvial
Marine
s/L = 0.45
20 km
F
Flow
direction
Downdrift
Updrift
1 km
Longshore current
G
Channel
thalweg splits
A'
A
Channel
thalweg splits
Elongated levee
Subaerial
mouth bars
Initial river
bed
Subaqueous
mouth bar

Figure 5

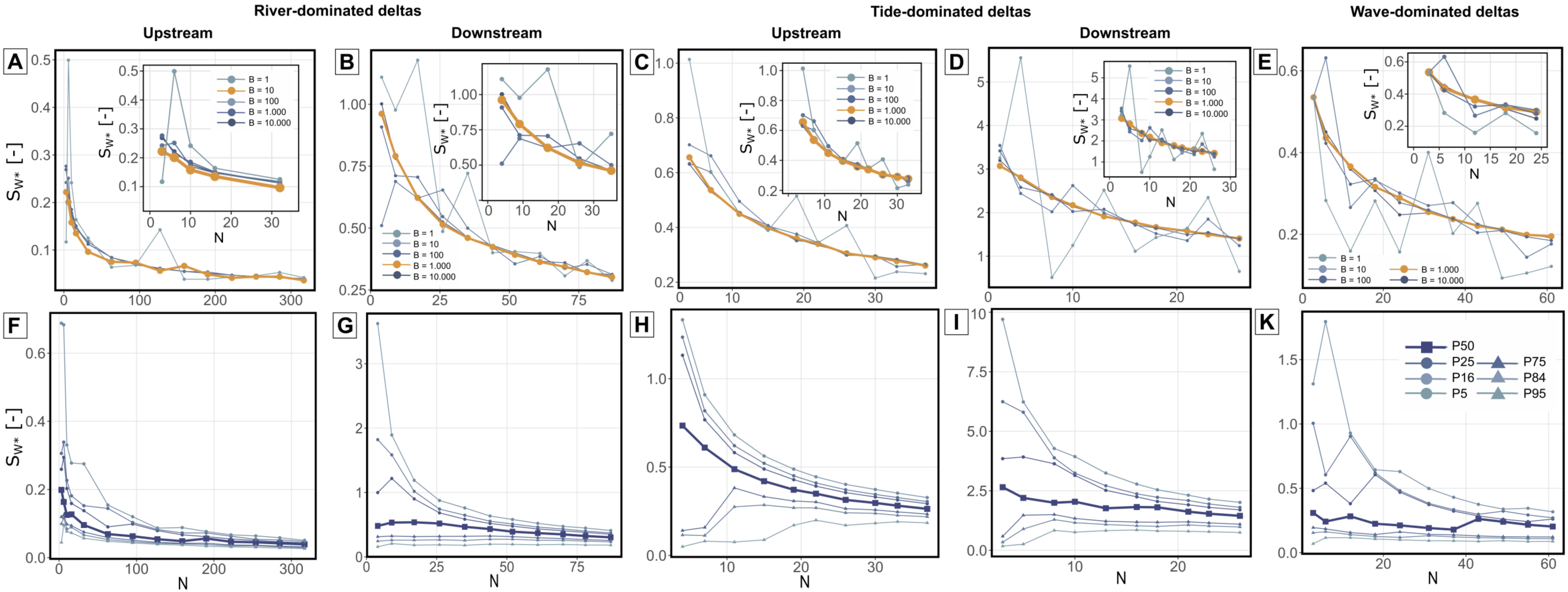

River-dominated deltas
Upstream
Downstream
Tide-dominated deltas
Upstream
Downstream
Wave-dominated deltas
A
B
C
D
E
F
G
H
I
K
B = 1
B = 10
B = 100
B = 1.000
B = 10.000
P50
P25
P16
P5
P75
P84
P95
S_{W^*} [-]
N

Figure 6

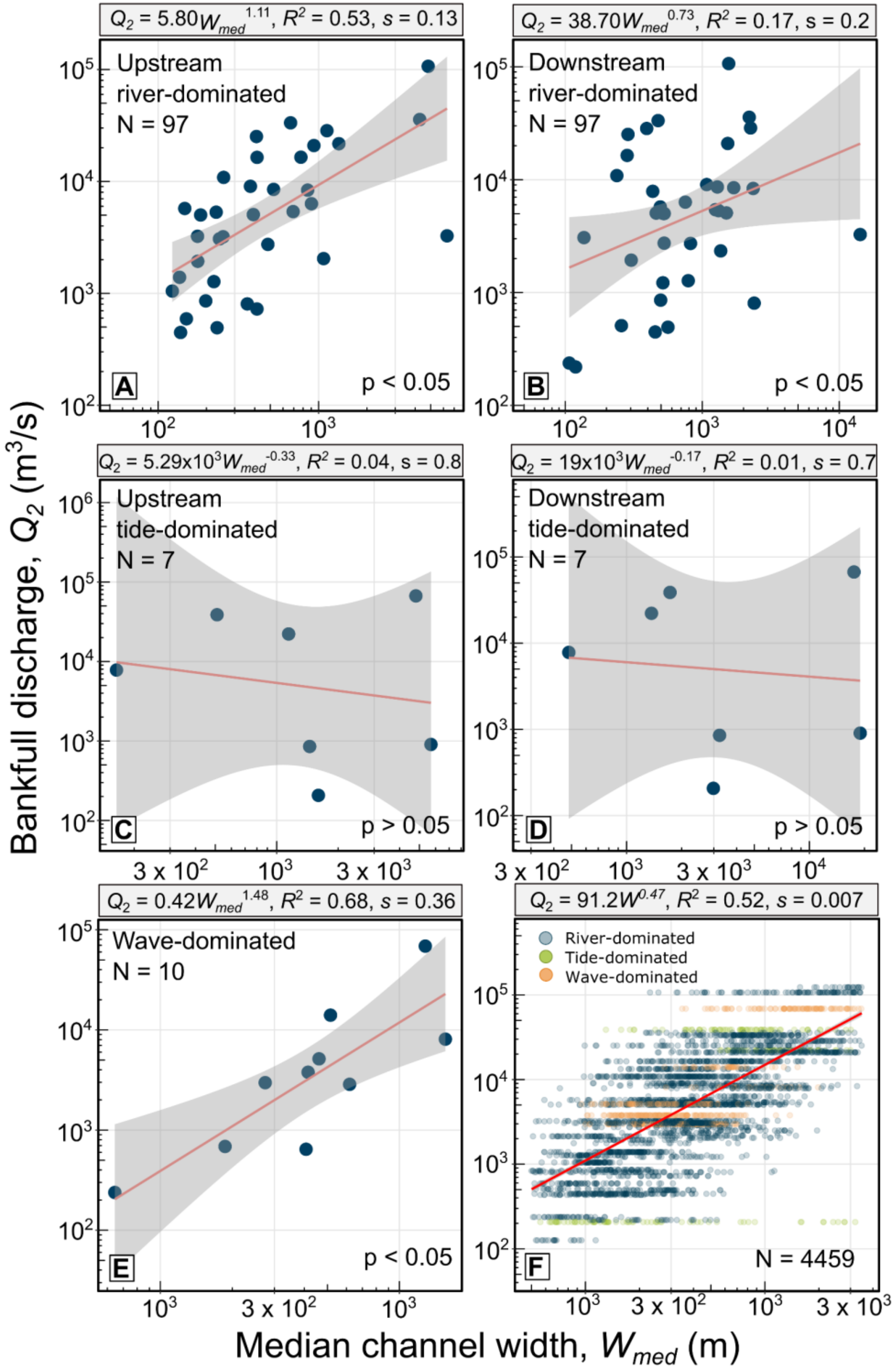

$Q_2 = 5.80W_{med}^{1.11}$, $R^2 = 0.53$, $s = 0.13$
Upstream river-dominated
N = 97
p < 0.05
A
$Q_2 = 38.70W_{med}^{0.73}$, $R^2 = 0.17$, $s = 0.2$
Downstream river-dominated
N = 97
p < 0.05
B
$Q_2 = 5.29\times10^3W_{med}^{-0.33}$, $R^2 = 0.04$, $s = 0.8$
Upstream tide-dominated
N = 7
p > 0.05
C
$Q_2 = 19\times10^3W_{med}^{-0.17}$, $R^2 = 0.01$, $s = 0.7$
Downstream tide-dominated
N = 7
p > 0.05
D
$Q_2 = 0.42W_{med}^{1.48}$, $R^2 = 0.68$, $s = 0.36$
Wave-dominated
N = 10
p < 0.05
E
$Q_2 = 91.2W^{0.47}$, $R^2 = 0.52$, $s = 0.007$
River-dominated
Tide-dominated
Wave-dominated
N = 4459
F
Bankfull discharge, Q_2 (m^3/s)
Median channel width, W_{med} (m)

Figure 7

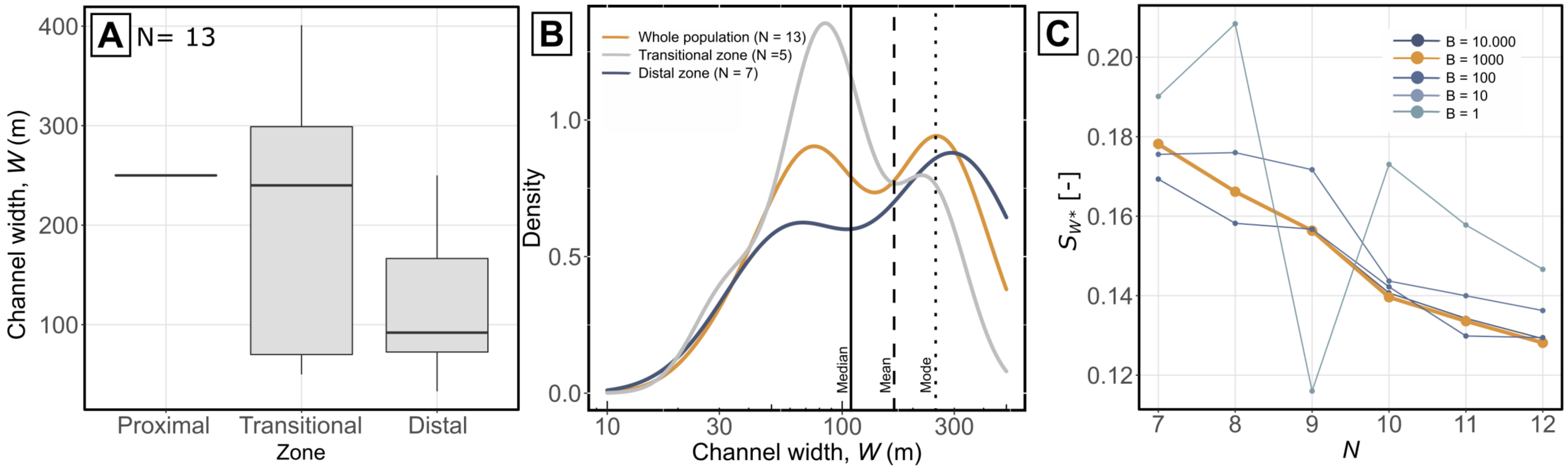

A
N= 13
400
300
200
100
Channel width, W (m)
Proximal
Transitional
Distal
Zone
B
Whole population (N = 13)
Transitional zone (N =5)
Distal zone (N = 7)
1.0
0.5
0.0
Density
Median
Mean
Mode
10
30
100
300
Channel width, W (m)
C
B = 10.000
B = 1000
B = 100
B = 10
B = 1
0.20
0.18
0.16
0.14
0.12
S_{W^*} [-]
7
8
9
10
11
12
N

Table 1.

Measured width (m)	Zone	Latitude	Longitude
250	Proximal	36.93349	-103.62979
401	Transitional	35.49859	-103.81257
299	Transitional	35.53891	-103.84624
240	Transitional	35.53491	-103.86028
70	Transitional	35.54482	-103.84091
50	Transitional	35.53751	-103.84859
71	Distal	34.991298	-103.396205
92	Distal	34.991222	-103.41928
109	Distal	34.91677	-103.49411
33	Distal	34.86206	-103.54559
224	Distal	34.937565	-103.469176
74	Distal	34.93272	-103.48047
250	Distal	34.99736	-103.38935

Supporting Information

Data bias induced by different data frequency

The semicircular method proposed by Sassi et al. (2012) provides consistent measured channel width frequency along a delta axis. Nonetheless, when being compared to other deltas with different sizes, data frequency becomes less consistent across deltas. This was due to the method centralizes the avulsion length and channel width as the basis of creating the semicircular grid. By having different avulsion length and channel width, each delta will have its unique semicircular grid sizes.

For example, if a delta has channel width at delta apex as 100 meter wide and avulsion length as 100-kilometer-long, the s/L could have the range of values from 0-1 with each semicircular will have a radius distance from the apex for every $s/L = 0.01$ that will produce 100 width measurement points for this delta. But imagine a delta with 50 meter wide at the delta apex with 10-kilometer-long avulsion length. The semicircular grid will have a radius distance from the apex for every $s/L = 0.05$ that will produce 20 width measurement points for this delta. For these two deltas, the data frequency will be 100 and 20, consecutively.

To mitigate this, different data binning frequencies were deployed to see their impacts on inducing the bias in defining the upstream and downstream channel width pattern. The original data (upper row in Fig. S1) show too frequent boxplots with high variance. The along delta axis data that are too frequent makes them difficult to see the changing pattern of channel width from upstream to downstream. By having 10% data binning frequency from its original data, the upstream to downstream profile shows less variance in channel width distribution, making it easier to see the changes of channel width along the axis (middle row in Fig. S1). In contrast, reducing the data frequency too much (i.e. 20% from original data) may lead to the data scarcity, obscuring the pattern between the upstream and downstream channel widths (lowermost row in Fig. S1).

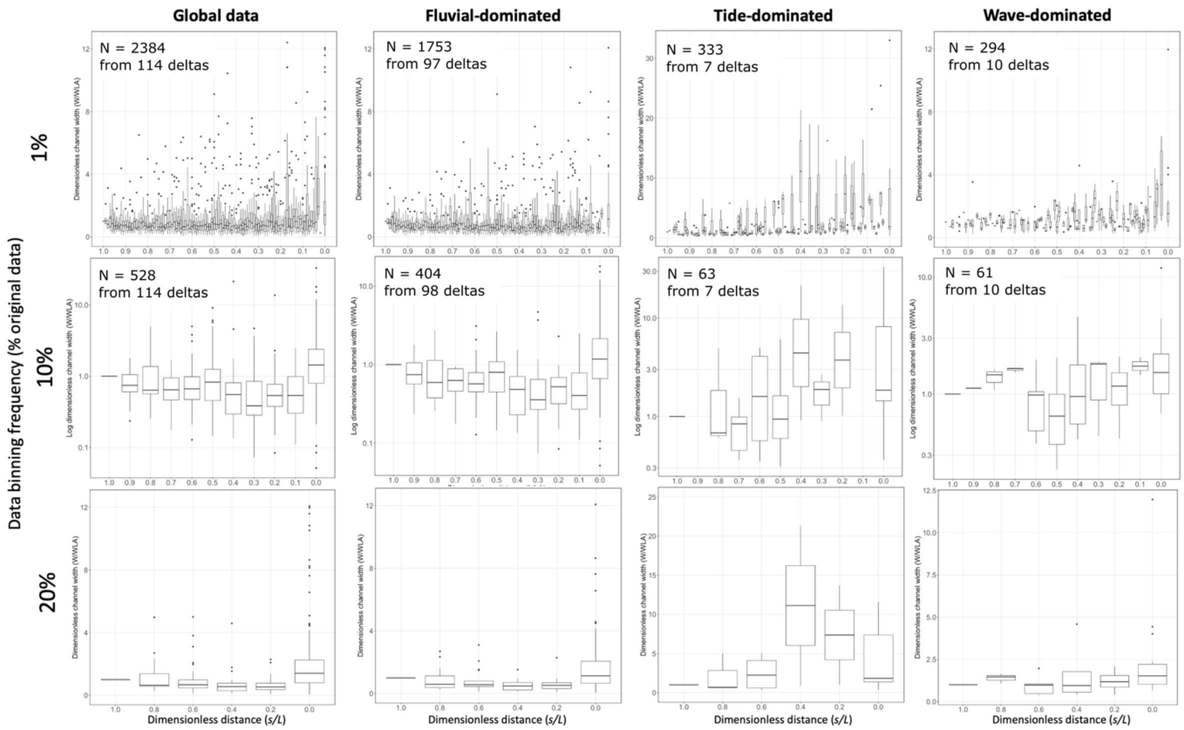

Figure S1. Different data binning frequency across global dataset (first column), fluvial-dominated (second column), tide-dominated (third column) and wave-dominated deltas (fourth column). The 10% data binning frequency were chosen as the basis of upstream-downstream channel width classification due to its less noise/variance along the delta axis in comparison to 1% and 20% data binning frequency.

Monthly-discharge transformation

Bankfull discharge is considered the controlling factor of channel geometry ((De Rose *et al.*, 2008; Haucke & Clancy, 2011; Gleason, 2015). Bankfull discharge is considered from the daily discharge dataset (GRDC) as Q_2, where 2 is the recurrence interval (years) of the discharge, as also used by Eaton, 2013; Jacobsen & Burr, 2016; Morgan & Craddock, 2019. Nonetheless, the river discharge dataset available from the Global Runoff Data Centre (GRDC), only provides discharge data for 75 of the 114 selected deltas in this study. Daily discharge is available for 56 of these 75. Monthly discharge data for the other 19 deltas needs to be transformed per climate to obtain the bankfull discharge values. To ensure comparability between the sites with daily and monthly flow data, transfer functions were calculated for each climate. As flow duration characteristics are climate-dependent, we adopted the Köppen-Geiger climate classification for this transformation (Beck et al., 2018).

For both the daily and monthly discharge datasets, the 2-year recurrence interval flows (Q_{2daily} and $Q_{2monthly}$) were calculated using The Flow Analysis Summary Statistics Tool for R ('fasstr' package). Q_{2daily} and $Q_{2monthly}$ were used to generate transfer functions using ordinary least square (OLS) regression for each climate zone (Fig. S2; Burgers et al., 2014). The resulting relationships provide the input to obtain the 2-year intervals or bankfull water discharge for the 19 sites with only monthly discharge data available.

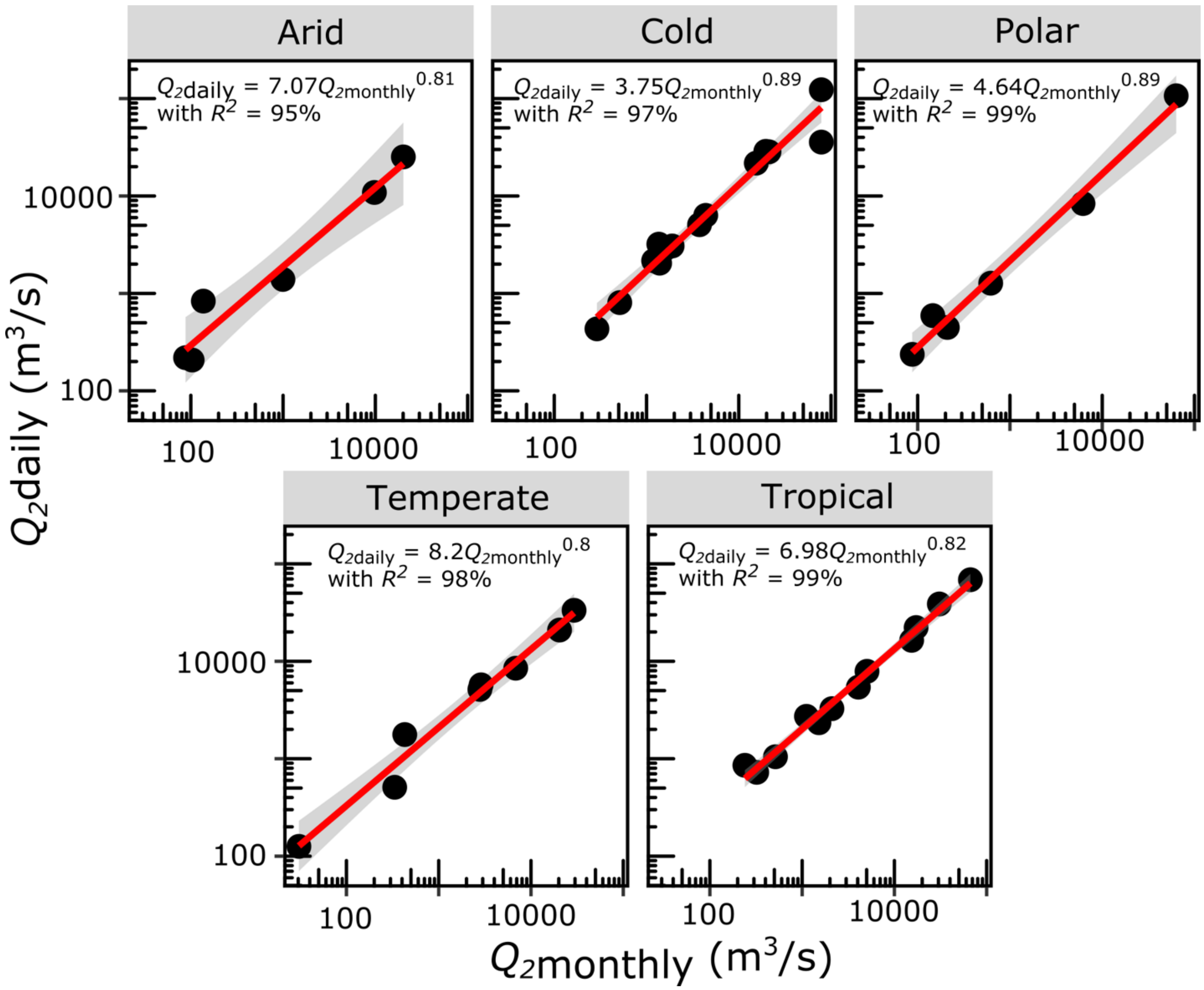

Figure S2. Transform function between monthly and daily discharge per climate. When only the monthly discharge data are available, 2-year recurrence interval (Q_2) or bankfull water discharge is obtained from the transform function applied to each climate.

Lower Mesa Rica paleodischarge estimation using the Fulcrum method

The Fulcrum method is originally proposed by Holbrook & Wanas (2014) to estimate basin-fill water and sediment volumes over geologic time. The main assumption used is that the water and sediment mass collected and transported by the rivers from a catchment should be in balance with the mass deposited in the basin. Also, the Fulcrum method does not require assumptions about the source catchment area and longitudinal trends (e.g. grain size and geometry change) within the fluvial system (Holbrook & Wanas, 2014) as in other methods (e.g. BQART; Syvitski & Milliman, 2007; trunk-based model; Bhattacharya et al., 2016; regional hydraulic geometry curves; Davidson & North, 2009). The Fulcrum method also limits the use of single paleochannel (i.e. trunk channel) that may be particularly difficult to be adapted to distributary system like in river deltas (Holbrook & Wanas, 2014). The compilation of previously published data is used in this study to calculate the bankfull paleodischarge (*Qbf* or Q_2 in this study) of the lower Mesa Rica trunk channel using the Fulcrum method:

$$Q_{bf} = \sqrt{\frac{g{H_{bf}}^3 S{B_{bf}}^2}{C_f}} \tag{S1}$$

And

$${C_f}^{-\frac{1}{2}} = 8.32(\frac{{H_{bf}}^2}{k_s}) \tag{S2}$$

$$k_s = 3D_{90} + 1.1\Delta(1 - e^{-25\psi}) \tag{S3}$$

$$\Delta = \frac{h_{bf}}{8} \tag{S4}$$

$$\psi = \frac{\Delta}{\lambda} \tag{S5}$$

$$\lambda = 7.3h_{bf} \tag{S6}$$

With

g = gravitational acceleration (m^2/s) = 9.8 m^2/s

H_{bf} = average bankfull channel depth (m)

S = slope or paleoslope (dimensionless)

B_{bf} = bankfull channel width (m)

C_f = dimensionless Chezy friction coefficient

Δ = mean bedform height (m)

λ = bedform wavelength

Input values are listed in Table S1). The calculation for paleoslope is using an empirical equation (Holbrook & Wanas, 2014; Trampush et al., 2014):

$$\tau^*_{bf50} = \frac{H_{bf}S}{RD_{50}}$$

With

τ^*_{bf50} = bankfull Shields number for dimensionless shear stress; is assumed to be 1.86 (Holbrook & Wanas, 2014)

H_{bf} = average bankfull channel depth (m)

S = paleoslope

R = submerged density in water of standard density; assuming the sediment are quartz, the R becomes 1.65 g/cm^3

D_{50} = average grainsize for the lowermost portion of a channel; represents the coarsest material transported as bedload.

The bankfull paleodischarge values for the trunk channel (Q_{bf} = 1085-1392 m^3/s) is in the same order of magnitude with the bankfull paleodischarge values estimated based on distributary channels (i.e. 1010 m^3/s) using the models proposed in this study.

Table S1. Estimates of paleohydrologic parameters and discharge from the lower Mesa Rica Sandstone. H_{bf}, B_{bf} and D_{50} from Van Yperen et al. (2021).

Channel story name	Average bankfull channel depth, H_{bf} (m)	Bankfull channel width, B_{bf} (m)	D_{90} (mm)	D_{50} (mm)	Δ (m)	λ	S	k_s	Dimensionless Chezy friction coefficient (C_f)	Bankfull paleodischarge, Q_{bf} (m^3/s)
Corazon Hill	5.5	200	0.48	0.28	0.6875	40.15	0.00015624	0.26	0.005	1392
Canadian River	5.5	200	0.25	0.17	0.6875	40.15	0.00009486	0.26	0.005	1085
CR C15A	5.5	200	0.44	0.23	0.6875	40.15	0.00012834	0.26	0.005	1262
Red Tongue Mesa	5.5	200	0.34	0.22	0.6875	40.15	0.00012276	0.26	0.005	1235

84